DispatchDate: 11.02.2021 · ProofNo: 642, p.1

nature cell biology

ARTICLES

https://doi.org/10.1038/s41556-021-00642-9

Check for updates

AIDA directly connects sympathetic innervation to adaptive thermogenesis by UCP1

Meng Shi[1,5], Xiao-Yu Huang[1,5], Xin-Yi Ren[1], Xiao-Yan Wei[1], Yue Ma[1], Zhi-Zhong Lin[1], Dong-Tai Liu[1], Lintao Song[1], Tong-Jin Zhao[1], Guang Li[1], Luming Yao[1], Mingxia Zhu[1], Cixiong Zhang[1], Changchuan Xie[1], Yaying Wu[1], Han-Ming Wu[2], Li-Ping Fan[2], Jingxing Ou[3], Yi-Hong Zhan[2], Shu-Yong Lin[1,4]✉ and Sheng-Cai Lin[1]✉

The sympathetic nervous system–catecholamine–uncoupling protein 1 (UCP1) axis plays an essential role in non-shivering adaptive thermogenesis. However, whether there exists a direct effector that physically connects catecholamine signalling to UCP1 in response to acute cold is unknown. Here we report that outer mitochondrial membrane-located AIDA is phosphorylated at S161 by the catecholamine-activated protein kinase A (PKA). Phosphorylated AIDA translocates to the intermembrane space, where it binds to and activates the uncoupling activity of UCP1 by promoting cysteine oxidation of UCP1. Adipocyte-specific depletion of AIDA abrogates UCP1-dependent thermogenesis, resulting in hypothermia during acute cold exposure. Re-expression of S161A-AIDA, unlike wild-type AIDA, fails to restore the acute cold response in *Aida*-knockout mice. The PKA–AIDA–UCP1 axis is highly conserved in mammals, including hibernators. Denervation of the sympathetic postganglionic fibres abolishes cold-induced AIDA-dependent thermogenesis. These findings uncover a direct mechanistic link between sympathetic input and UCP1-mediated adaptive thermogenesis.

Maintaining body temperature within a narrow range by adaptive thermogenesis is a fundamental physiological feature in homeothermic organisms. Adaptive thermogenesis refers to heat generation in response to cold stress, which can be divided into shivering and non-shivering thermogenesis. Brown adipose tissue (BAT) is highly specialized for adaptive non-shivering thermogenesis conferred by uncoupling protein 1 (UCP1), a mitochondrial transmembrane protein that uncouples oxidative phosphorylation from ATP generation in the inner mitochondrial membrane[1–3]. It allows protons that have built up in the mitochondrial intermembrane space to return to the matrix side, providing a mechanism for the large heat-generating capacity of BAT[4]. Non-shivering thermogenesis endows a large number of mammals with the ability to withstand acute cold. It is particularly relevant to small mammalian hibernators that possess a large BAT mass, which enables rapid rewarming from hypothermic torpor periodically throughout the hibernation season[5]. *Ucp1*-knockout (KO) mice are sensitive to exposure to acute cold[6]. Interestingly, UCP1 seems to mainly function in the acute cold response because its deficiency does not affect animals that have undergone gradual adaptation[7,8].

Changes in body temperature, cardiac function, blood pressure and physical activity comprise the fight-or-flight response and can be critical for the survival of the organism during dangerous situations[9]. This process is mediated primarily by the sympathetic nervous system (SNS), particularly by the release of catecholamines, including epinephrine from the adrenal medulla and norepinephrine from sympathetic neurons[10]. Postganglionic sympathetic neurons release large quantities of norepinephrine into innervated BAT and other tissues after exposure to cold[11–13]. These catecholamines activate protein kinase A (PKA) via their respective adrenoreceptors. It is known that PKA influences the activity of UCP1 profoundly through the modulation of a variety of cellular events including the mobilization of stored fatty acids by enhancing lipolysis, secretion of adipokines and transcription of thermogenic genes, including *Ucp1* (refs. [14,15]).

Current models suggest that long-chain fatty acids released via PKA-stimulated lipolysis are essential for initiating the dissipation of a proton gradient by UCP1 (refs. [16–18]). On the other hand, under unstimulated conditions, purine nucleotides (primarily ATP) bind on the cytoplasmic side of UCP1 to inhibit proton transfer[19,20]. In addition, sulfenylation, one form of cysteine oxidation, has been found to be a critical post-translational modification of UCP1, which is triggered by a rise in reactive oxygen species (ROS) resulting from increased fatty-acid oxidation after adrenergic activation[21]. Lysine succinylation and acetylation have also recently been reported to modulate the function of UCP1 (ref. [22,23]).

However, no direct integrator(s) relaying the effect of SNS activation to physically act on UCP1 has been identified. Here we report that AIDA—a C2-domain-containing protein that antagonises diet-induced obesity by limiting the intestinal absorption of fat[24,25]—plays an essential role in cold-induced UCP1-dependent non-shivering thermogenesis in BAT. Mechanistically, AIDA acts as a direct substrate of PKA following adrenergic stimulation, with the phosphorylated residue mapped to S161. Phosphorylated AIDA interacts with UCP1 to promote its cysteine oxidation. Moreover, unlike wild-type (WT) AIDA, re-expression of the S161A-AIDA mutant into BAT of mice with whole-body KO of *Aida* (global *Aida* KO, *Aida*-GKO) fails to restore adaptive thermogenesis. These findings suggest that AIDA is a critical mediator receiving adrenergic signalling and relaying to UCP1 activation via direct interaction.

[1]State Key Laboratory of Cellular Stress Biology, School of Life Sciences, Xiamen University, Xiamen, China. [2]Department of Neurology, First Affiliated Hospital, Xiamen University, Xiamen, China. [3]Department of Hepatic Surgery and Liver Transplantation Centre of the Third Affiliated Hospital, Guangdong Province Engineering Laboratory for Transplantation Medicine, Guangzhou, China. [4]Department of Digestive Diseases, School of Medicine, Xiamen University, Xiamen, China. [5]These authors contributed equally: Meng Shi, Xiao-Yu Huang. ✉e-mail: linsy@xmu.edu.cn; linsc@xmu.edu.cn

Uncorrected Proofs

Results

AIDA is required for thermogenesis under cold stress. Mice with intestinal KO of *Aida* are less obese than those with *Aida*-GKO[24], suggesting that AIDA may have effects on energy balance in other systemic tissues apart from the intestine. Here we found that the rectal temperatures of *Aida*-GKO mice dropped more rapidly than their WT littermates during acute cold stress. After 4 h of cold challenge, the average body temperature of *Aida*-GKO mice was approximately 2 °C lower than that of WT mice (Fig. 1a). Increases in oxygen consumption and energy expenditure after cold exposure were also impaired in AIDA-deficient mice (Fig. 1b and Extended Data Fig. 1a). To investigate the contribution of AIDA in adipose tissue to this effect, *Aida* double-floxed (*Aida*$^{f/f}$) mice were crossed with *Adipoq–cre* mice to generate offspring with adipocyte-specific knockout of *Aida* (*Aida*-AKO; Extended Data Fig. 1b). Like *Aida*-GKO mice, *Aida*-AKO mice were more sensitive to cold (Fig. 1c) and showed reduced cold-induced thermogenesis (Fig. 1d and Extended Data Fig. 1c), although they had a similar body weight, body composition (lean and fat mass), oxygen consumption and energy expenditure under normal conditions (Fig. 1e–g and Extended Data Fig. 1d). Together, these results reveal that AIDA plays a critical role in cold-induced thermogenesis in adipose tissue.

AIDA mediates activation of thermogenesis by the SNS in BAT. We next investigated whether AIDA mediates the thermogenic effects of adrenergic signalling from the SNS. We blocked sympathetic stimulation to BAT by surgical denervation in the intrascapular BAT of mice. Denervation of WT mice caused a similar decline in adaptive thermogenesis and body temperature to that of *Aida*-GKO mice after acute cold exposure; there were no differences in body temperature, rates of oxygen consumption or energy expenditure between denerved WT and denerved *Aida*-GKO mice (Fig. 2a,b and Extended Data Fig. 2a). In addition, after pretreatment with the β-adrenergic blocker SR59230A or propranolol, no difference in body-temperature decline after acute cold stress was seen between *Aida*$^{f/f}$ and *Aida*-AKO mice (Fig. 2c and Extended Data Fig. 2b). Notably, no differences in the levels of neuronal-specific TUBB3 or the abundance and activational phosphorylation of tyrosine hydroxylase (TH, a rate limiting enzyme in catecholamine synthesis) were observed in the BAT from *Aida*-AKO and *Aida*$^{f/f}$ mice (Extended Data Fig. 2c). We also injected mice with a selective β3-adrenergic receptor agonist, CL316243, which mimics sympathetic input into adipose tissue. Although CL316243-treated WT mice showed an increase in the dorsal surface temperature of the interscapular area[26], such a response was absent in *Aida*-GKO mice (Fig. 2d). Importantly, the oxygen-consumption rates (OCR) and energy expenditure of *Aida*-AKO mice were lower than *Aida*$^{f/f}$ mice following CL316243 injection (Extended Data Fig. 2d,e). In addition, AIDA depletion in cultured primary brown adipocytes led to a significant reduction in uncoupling respiration induced by isoproterenol (ISO), a β-adrenoceptor agonist (Fig. 2e). Like *Aida*-AKO mice, mice with BAT-specific knockout of *Aida* (*Aida*-BKO) showed intolerance to acute cold without a change in body composition (Fig. 2f and Extended Data Fig. 2f,g), indicating that it is the BAT that is modulated by AIDA in acute cold response.

To further ascertain the specific role of AIDA in the acute cold response, we measured a series of parameters in stepwise cold-adapted mice. Except for body weight, which is attributed to higher intestinal absorption of fat in *Aida*-GKO mice, as shown previously[24], no differences were observed between *Aida*-GKO mice and their control littermates (Extended Data Fig. 3a–g). These findings demonstrate that AIDA is not required for the defence of body temperature or energy metabolism during long-term cold adaptation.

Phosphorylation of AIDA by PKA promotes adaptive thermogenesis. The strong link between AIDA and adrenergic signalling led us to test for possible direct phosphorylation of AIDA. We found that norepinephrine and epinephrine, but not dopamine, induced AIDA phosphorylation in brown adipocytes, as demonstrated by Phos-tag gels, in which mobility-impeded protein bands represent phosphoproteins (Fig. 3a and Extended Data Fig. 4a,b). The mobility-impeded band of AIDA was then extracted and subjected to mass spectrometry analysis, revealing that AIDA is phosphorylated at S161 (Extended Data Fig. 4c). Next, polyclonal antibody that specifically recognizes phosphorylated S161 on AIDA was raised. AIDA was phosphorylated when co-expressed with the WT, but not the kinase-dead, form of PKA (Extended Data Fig. 4d). The phosphorylation of AIDA was blocked by a S161A mutation (Fig. 3b). Treatment of the immunoprecipitated WT-AIDA with calf-intestinal alkaline phosphatase eliminated the phosphorylation (Extended Data Fig. 4e). We also found that the forskolin-stimulated phosphorylation of AIDA was diminished after treatment with the PKA inhibitor H89—but not with inhibitors of other kinases, including AMPK, Aurora B and AKT (Extended Data Fig. 4f). An in vitro kinase assay confirmed that PKA could directly phosphorylate AIDA on S161 (Fig. 3c). Importantly, the levels of S161-phosphorylated AIDA and the interaction between AIDA and PKA were substantially increased in the BAT of cold-exposed or adrenergic-stimulated mice (Fig. 3d and Extended Data Fig. 4g).

We next studied the biological relevance of the phosphorylation of AIDA in adaptive thermogenesis. The adeno-associated virus (AAV) system was used to deliver green fluorescent protein (GFP; as a control), WT-AIDA or the mutants S161A-AIDA or S161D-AIDA back into *Aida*-GKO mice via injection into the tail vein. The injected vectors expressed the respective proteins exclusively in BAT via the mini-promoter and enhancer of *Ucp1* (refs. [27–29]; Extended Data Fig. 5a). Introduction of WT-AIDA, but not the rest, into the BAT of *Aida*-GKO mice rescued the decrease in body temperature and adaptive thermogenesis (Fig. 3e,f and Extended Data Fig. 5b). Together, these results strongly suggest that phosphorylation of AIDA on S161 is a key event triggering thermogenesis in BAT.

AIDA-mediated adaptive thermogenesis depends on UCP1. We performed knockdown (KD) of *Ucp1* by AAV-based small-interfering-RNA-mediated gene silencing to investigate whether AIDA exerts its role in adaptive thermogenesis through UCP1 (Fig. 4a). The body temperatures of the *Ucp1*-depleted *Aida*$^{f/f}$ mice declined rapidly during acute cold exposure. However, compared with the mice expressing control siRNA, a deficiency of AIDA in the *Ucp1*-KD mice did not exhibit further decreased adaptive thermogenesis when exposed to cold (Fig. 4b,c and Extended Data Fig. 6a) or stimulated with CL316243 (Fig. 4d and Extended Data Fig. 6b). Similarly, some of the electron-transport-chain components—NDUFV2, SDHA, UQCRC2 and COX4—showed similar reduction in *Ucp1*-KD BAT regardless of the presence of AIDA (Fig. 4e). Notably, no differences were detected in the messenger RNA or protein levels of UCP1 in BAT of WT and *Aida*-GKO mice before and after cold exposure or CL316243 treatment (Fig. 4f,g and Extended Data Fig. 6c–f), indicating that the reduced thermogenesis in *Aida*-GKO mice cannot be attributed to decreased UCP1 levels.

We previously found that intestinal AIDA is associated with endoplasmic reticulum-associated degradation (ERAD)[24]. ERAD has been reported to influence thermogenesis by controlling mitochondrial dynamics in BAT from mice that have been exposed to cold[30]. Thus, we compared ERAD-associated proteins in the BAT of *Aida*$^{f/f}$ and *Aida*-AKO mice under cold stress. However, we found that GPAT3, MOGAT2 and DGAT2 as well as SIGMAR1, an indicator of cold-induced ERAD[30], were unaffected in BAT by *Aida* knockout (Extended Data Fig. 6g), suggesting that AIDA-dependent ERAD activity does not play a role in BAT.

Uncorrected Proof

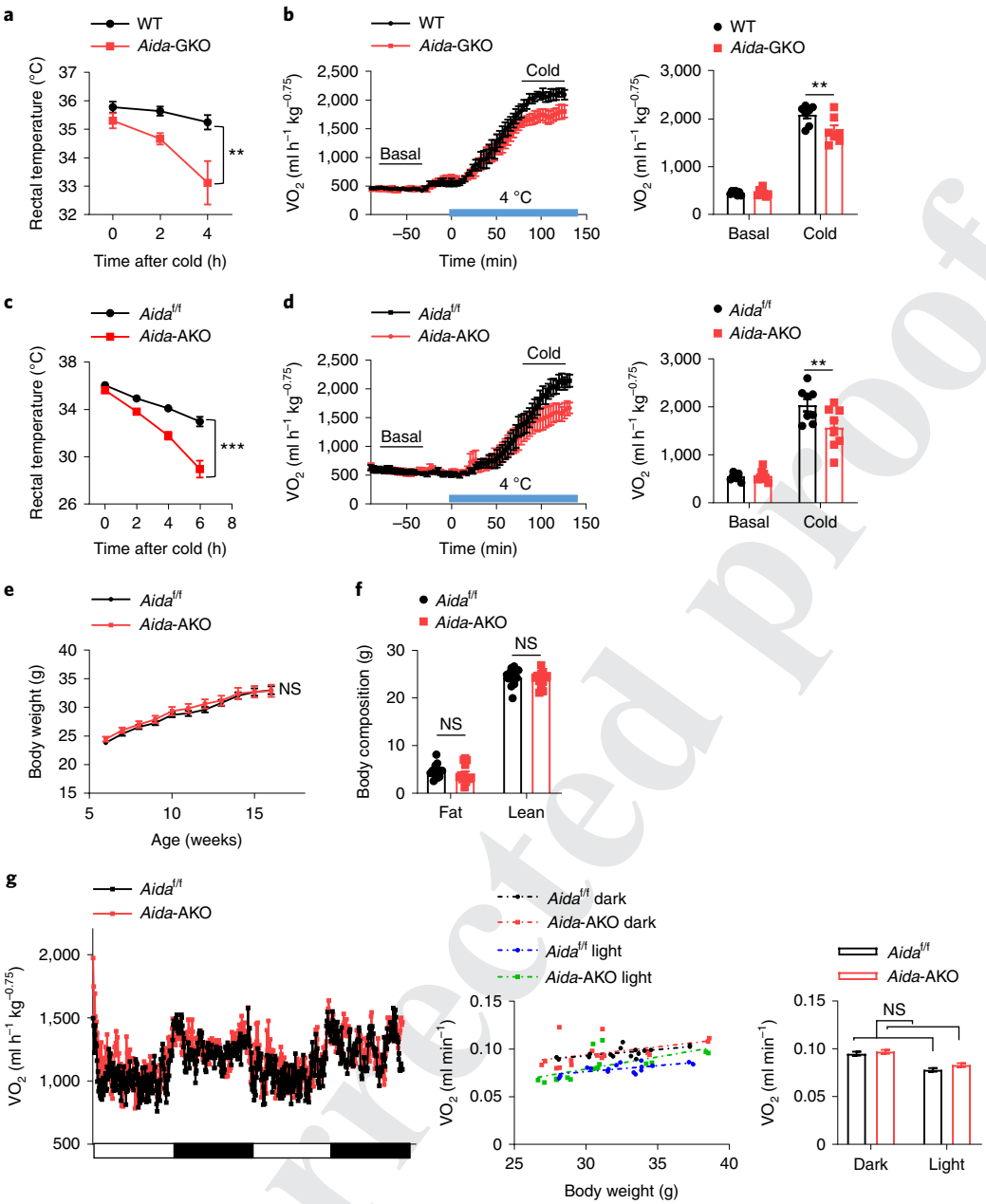

Fig. 1 | AIDA is required for thermogenesis under cold stress. a, Cold tolerance test (CTT) of WT and *Aida*-GKO mice. Data are the mean ± s.e.m.; $n = 8$ mice per group. $^{**}P = 0.0046$, two-way repeated-measure analysis of variance (RM ANOVA) with Geisser–Greenhouse's correction. **b**, OCR (VO_2) of WT and *Aida*-GKO mice under acute cold exposure. Data were collected from $n = 7$ mice per group and are expressed as the mean ± s.e.m. of values normalized to the body weight ($kg^{0.75}$; left) or individual values with the mean ± s.e.m. of the average OCR under basal and cold conditions (right). $^{**}P = 0.0046$, two-way RM ANOVA with Sidak. The basal-level OCR was calculated as the average of 30–60 min before the shift in ambient temperature; the OCR under cold conditions was calculated as the average of 100–130 min after the temperature shift. **c**, CTT of $Aida^{f/f}$ and *Aida*-AKO mice. Data are the mean ± s.e.m.; $Aida^{f/f}$, $n = 7$ and *Aida*-AKO, $n = 12$. $^{***}P = 0.0002$, two-way RM ANOVA with Geisser–Greenhouse's correction. **d**, OCR of $Aida^{f/f}$ and *Aida*-AKO mice under acute cold exposure. Data were collected from $n = 8$ mice per group and are expressed as the mean ± s.e.m. of values normalized to the body weight ($kg^{0.75}$; left) or individual values with the mean ± s.e.m. of the average OCR under basal and cold conditions (right). $^{**}P = 0.0064$, two-way RM ANOVA with Sidak. The basal OCR was calculated as the average of the 30–60 min before the shift in ambient temperature; the OCR under cold was calculated as the average of 100–130 min after the temperature shift. **e**,**f**, Body weight (**e**) and body composition (**f**) of mice on a chow diet. The fat mass and the lean mass of 16-week-old mice were measured. The effect of genotype on body weight is considered not significant (**e**; NS; two-way RM ANOVA with Geisser–Greenhouse's correction). Data of $n = 14$ mice per group are shown as the mean ± s.e.m.; two-way RM ANOVA with Sidak. **g**, OCR of female mice on a chow diet housed at room temperature (24 °C). Data were collected from $n = 8$ mice per group for 2 d and are expressed as the mean of values normalized to the body weight ($kg^{0.75}$; left), the individual OCR under dark or light phases (middle) and the adjusted mean ± s.e.m. based on a normalized mouse weight of 31.8610 g determined using ANCOVA (right). Left: the white and black bars along the bottom correspond to the light and dark cycles, respectively. $^{**}P < 0.005$; $^{***}P < 0.0005$; IB, immunoblot. Numerical source data are provided.

Uncorrected proofs

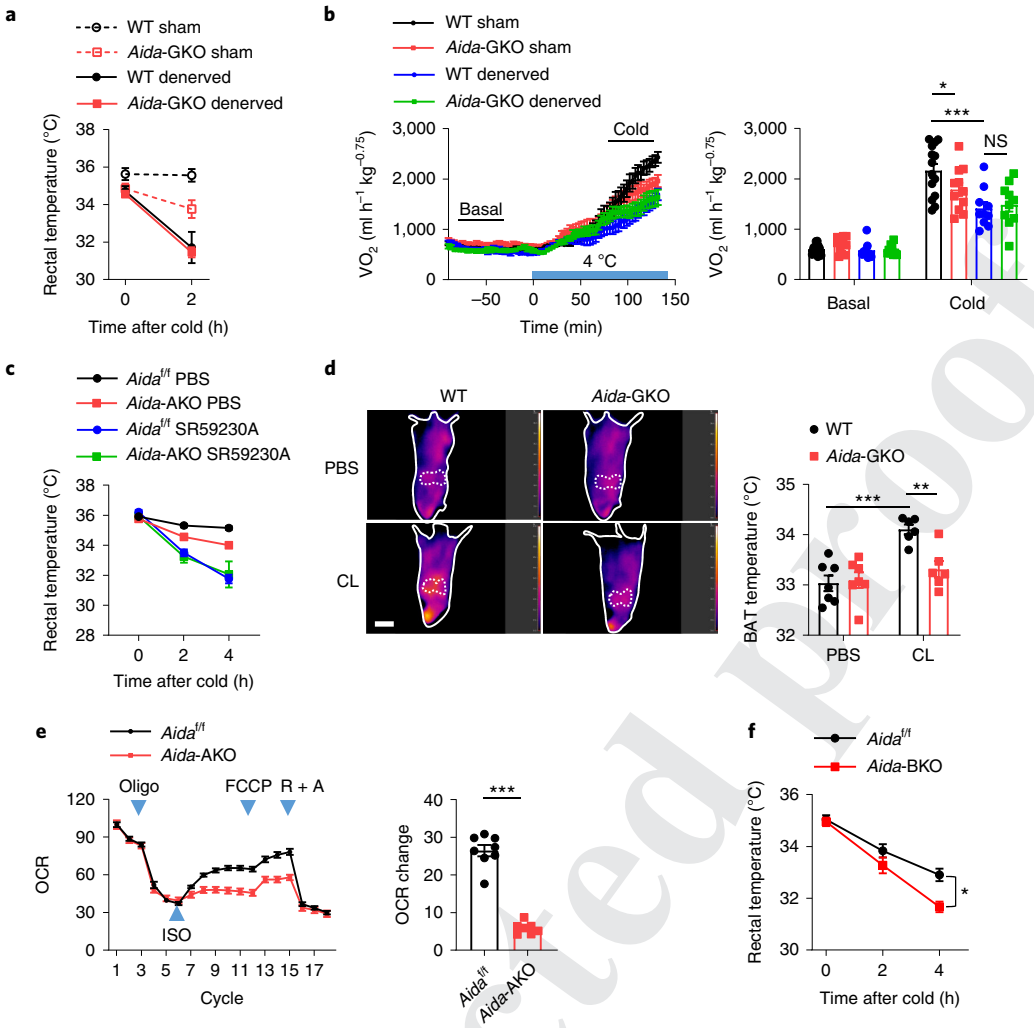

Fig. 2 | AIDA is required for sympathetic activation of BAT. a, CTT of mice 2 weeks after denervation. Data are the mean ± s.e.m.; $n = 9$ mice. WT sham versus *Aida*-GKO sham, $^{*}P = 0.0437$; WT sham versus WT denerved, $^{***}P < 0.0001$; WT denerved versus *Aida*-GKO denerved, $P > 0.9999$; two-way RM ANOVA with Sidak. **b**, OCR of the mice in **a** under acute cold. WT sham, $n = 14$; *Aida*-GKO sham, $n = 11$; WT denerved and *Aida*-GKO denerved, $n = 10$. Data are the mean ± s.e.m. of values normalized to the body weight ($kg^{0.75}$; left) or mean ± s.e.m. of the average OCR under basal and cold conditions (right). Basal OCR, average of 30–60 min before the shift in ambient temperature; cold-stimulated OCR, average of 100–130 min after the temperature shift. WT sham versus WT denerved, $^{***}P < 0.0001$; WT sham versus *Aida*-GKO sham, $^{*}P = 0.0323$; WT denerved versus *Aida*-GKO denerved, $P = 0.9554$; two-way RM ANOVA with Tukey. **c**, CTT of female mice pretreated with 5 mg kg^{-1} SR59230A. Data are the mean ± s.e.m. $Aida^{f/f}$ PBS and *Aida*-AKO SR59230A, $n = 10$; *Aida*-AKO PBS, $n = 8$; $Aida^{f/f}$ SR59230A, $n = 9$. $Aida^{f/f}$ PBS versus *Aida*-AKO PBS, $^{***}P < 0.0001$; two-way RM ANOVA with Geisser–Greenhouse's correction, followed by Tukey. **d**, Infrared images of anaesthetized mice that were intraperitoneally (i.p.) injected with PBS ($n = 7$ mice) or 1 mg kg^{-1} CL316243 (CL; $n = 6$ mice; left). The dashed lines indicate the iBAT regions. Temperatures of the BAT are shown as the mean ± s.e.m. (right). $^{**}P = 0.0072$, $^{***}P = 0.0002$; ordinary two-way ANOVA with Tukey. Scale bar, 2 cm. **e**, OCR of the brown adipocytes of the mice. Data are the mean ± s.e.m. For each cycle, the OCR is shown as the percentage of the initial OCR (left). Adipocytes were obtained from $n = 8$ $Aida^{f/f}$ and $n = 7$ *Aida*-AKO mice. Changes in ISO-induced OCRs relative to the basal mitochondrial uncoupling respiration rates as a percentage of the initial (right). $^{***}P < 0.0001$, two-tailed unpaired Student's *t*-test with Welch's correction. Oligo, oligomycin; R + A, rotenone and antimycin-A. **f**, CTT of *Aida*-BKO mice. Data are the mean ± s.e.m. $Aida^{f/f}$, $n = 16$; *Aida*-BKO, $n = 12$. $^{*}P = 0.0290$, two-way RM ANOVA with Geisser–Greenhouse's correction. $^{*}P < 0.05$; $^{**}P < 0.005$; $^{***}P < 0.0005$; NS, not significant. Numerical source data are provided.

AIDA interacts with UCP1. We next explored the mechanism of how AIDA modulates the function of UCP1 by initially examining the direct interaction between AIDA and UCP1. The interaction between overexpressed AIDA and UCP1 was increased in HEK293T cells after adrenergic stimulation (Fig. 5a). Moreover, endogenous AIDA and UCP1 showed increased interaction in BAT after cold exposure or adrenergic stimulation (Fig. 5b and Extended Data Fig. 7a). The mitochondrial localization of UCP1 prompted us to investigate the dynamics of the subcellular localization of AIDA. Immunofluorescence staining and fractionation assays showed a strong colocalization of AIDA with UCP1 in brown adipocytes (Extended Data Fig. 7b,c). As AIDA is targeted to cellular membranes with its C2 domain[25], we next performed detergent-free immunoprecipitation using BAT from mice transduced with *AAV–haemagglutinin (HA)–Aida*, in which the organelles remained intact (Fig. 5c). Mitochondrial marker proteins (VDAC, TOM20 and TIM23) were detected in the AIDA immunoprecipitates from unstressed BAT, indicating that AIDA is localized on the outer mitochondrial membrane under unstressed conditions. Acute cold exposure led to a dramatic reduction in the immunoprecipitated

Uncorrected Proofs

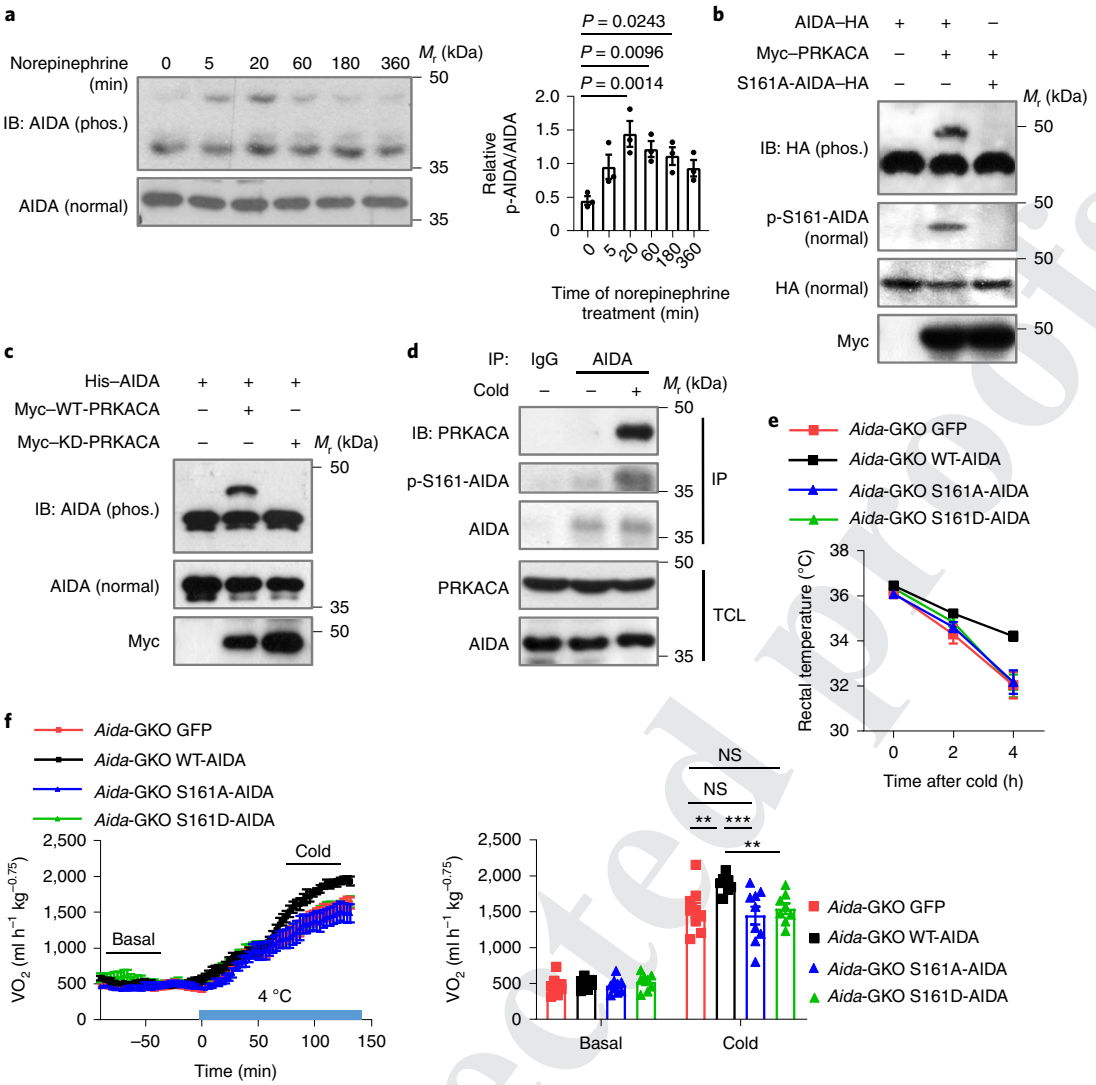

Fig. 3 | Phosphorylation of AIDA by PKA promotes adaptive thermogenesis. a, AIDA phosphorylation after norepinephrine stimulation. Brown adipocytes were treated with 1 μM norepinephrine. Cell extracts were analysed using Phos-tag or normal gels (left). The intensities of phosphorylated (p-AIDA) relative to total AIDA are quantified from three independent experiments and shown as the mean ± s.e.m. (right). Ordinary one-way ANOVA with Dunnett's test. **b**, A single mutation eliminates the phosphorylation of AIDA by PKA. HEK293T cells were co-transfected with PRKACA and HA-tagged WT-AIDA or S161A-AIDA. The total cell lysates (TCL) were subjected to immunoprecipitation against HA, followed by immunoblotting. AIDA phosphorylation of AIDA was analysed using Phos-tag gels or a phospho-site-specific antibody. **c**, Direct phosphorylation of AIDA by PKA. Mixtures containing Myc-tagged WT (Myc-WT-PRKACA) or kinase-dead (Myc-KD-PRKACA) PRKACA together with bacterially expressed histidine (His)-tagged AIDA were incubated, followed by Phos-tag gel analysis. **d**, Cold exposure increases endogenous AIDA-S161 phosphorylation. The BAT from mice exposed to 4 °C for 3 h were homogenized and subjected to immunoprecipitation against AIDA. **b**–**d**, Blots are representative examples of two independent experiments with similar results. IP, immunoprecipitation; IB, immunoblot; phos., Phos-tag gel. **e**, CTT of *Aida*-GKO mice after re-expression of AIDA or GFP, as a control, mediated by a *Ucp1* mini-promoter and enhancer-driven AAV. Data are the mean ± s.e.m.; $n = 12$ mice. *Aida*-GKO GFP versus *Aida*-GKO WT-AIDA, $^{*}P = 0.0168$; *Aida*-GKO WT-AIDA versus *Aida*-GKO S161A-AIDA, $^{*}P = 0.0146$; *Aida*-GKO WT-AIDA versus *Aida*-GKO S161D-AIDA, $^{**}P = 0.0061$; two-way RM ANOVA with Geisser–Greenhouse's correction, followed by Tukey. **f**, OCR of the mice in **e** under cold conditions. *Aida*-GKO GFP and *Aida*-GKO S161A-AIDA, $n = 9$; *Aida*-GKO WT-AIDA and *Aida*-GKO S161D-AIDA, $n = 8$. Data are the mean ± s.e.m. of values normalized to the body weight ($kg^{0.75}$; left) or individual values with the mean ± s.e.m. of the average OCR under basal and cold conditions (right). Basal OCR, average of 30–60 min before the shift in ambient temperature; cold-stimulated OCR, average of 100–130 min after the temperature shift. *Aida*-GKO GFP versus *Aida*-GKO WT-AIDA, $^{**}P = 0.0028$; *Aida*-GKO WT-AIDA versus *Aida*-GKO S161A-AIDA, $^{***}P = 0.0002$; *Aida*-GKO WT-AIDA versus *Aida*-GKO S161D-AIDA, $^{**}P = 0.0075$; two-way RM ANOVA with Tukey. $^{**}P < 0.005$; $^{***}P < 0.0005$; NS, not significant. Uncropped blots for **a**–**d** and numerical source data for **a**,**e**,**f** are provided.

AIDA as well as the mitochondrial marker proteins, whereas their total levels remained unchanged (Fig. 5d). As the total AIDA was not reduced in the mitochondrial fraction following adrenergic stimulation (Extended Data Fig. 7c), the reduction in AIDA and the mitochondrial markers in the immunoprecipitates from the detergent-free lysates indicate that acute cold promotes the translocation of AIDA from the outer membrane to inside the mitochondrial membrane. Importantly, S161A-AIDA and mitochondrial marker proteins remained unchanged in a similar assay (Fig. 5e). To visualize the sub-mitochondrial localization of AIDA in vivo, we

Uncorrected Proofs

expressed APEX2-tagged AIDA in AIDA-deficient mice via AAV injection (Extended Data Fig. 7d) and determined the localization of APEX2, an electron microscopy tag[31]. Strong APEX2 signals were seen in the mitochondrial intermembrane space in brown adipocytes from cold-exposed mice expressing APEX2–WT-AIDA but not APEX2–S161A-AIDA (Fig. 5f). Consistent with this result, the S161A AIDA mutation abrogated the adrenergic-induced interaction between AIDA and UCP1 (Fig. 5g). We next investigated the interfaces of the AIDA–UCP1 interaction. It was found that the region of amino acids 105–205 of AIDA, which encompasses S161, is responsible for the interaction with UCP1 (Extended Data Fig. 7e). Full-length UCP1 and various truncations retaining any two of the three repeated mitochondrial carrier domains could still interact with AIDA (Extended Data Fig. 7f). Together, these findings indicate that adrenergic-induced phosphorylation of AIDA promotes its translocation and direct interaction with UCP1.

Alignment of AIDA from different species shows that the S161 residue in mouse AIDA and the flanking amino-acid residues are highly conserved in vertebrates (Extended Data Fig. 7g). However, this serine has been replaced by proline in *Branchiostoma floridae*, one of the cephalochordates that are the closest living relatives of vertebrates. Alteration of P163 to serine in AIDA from *B. floridae* allows it to be phosphorylated by PKA (Extended Data Fig. 7h), suggesting a gain-of-function mutation of AIDA during the evolution of the vertebrates. In contrast, the PKA–AIDA–UCP1 axis is highly conserved in hibernating mammals, including marmots, hedgehogs and hamsters (Extended Data Fig. 7i–l).

AIDA enhances oxidative modification of UCP1. Induction of sulfenylation, one kind of cysteine oxidation, on UCP1 by increased ROS following acute cold stimulation has been shown to support adaptive thermogenesis[21]. Thus, we examined UCP1 oxidation by employing a redox gel-shift method[32]. Following acute cold exposure, cysteine oxidation on UCP1 was increased in WT but not *Aida*-GKO mice (Fig. 6a). Moreover, re-expression of WT AIDA, but not the S161A-AIDA, in *Aida*-GKO mice increased cold-induced UCP1 oxidation (Fig. 6b), indicating that AIDA phosphorylation is required for the ROS-mediated oxidative modification of UCP1.

We also found that the acute increase in the ROS levels in norepinephrine-treated brown adipocytes was similar between *Aida*$^{f/f}$ and *Aida*-AKO cells (Fig. 6c). Consistent with these results, AIDA depletion did not affect the protein levels of NRF2, the master regulator of the antioxidant response, or its target GCLC in the BAT of the mice exposed to acute cold (Fig. 6d). Moreover, the mitochondrial respiratory chain in BAT lacking AIDA showed comparable protein abundance of the mitochondrial complexes I–V (Fig. 6d). However, *N*-acetyl cysteine (NAC) pretreatment to inhibit protein thiol oxidation markedly reduced AIDA-dependent thermogenesis after exposure to acute cold or adrenergic stimulation (Fig. 6e,f and Extended Data Fig. 8a), indicating that ROS-induced protein thiol

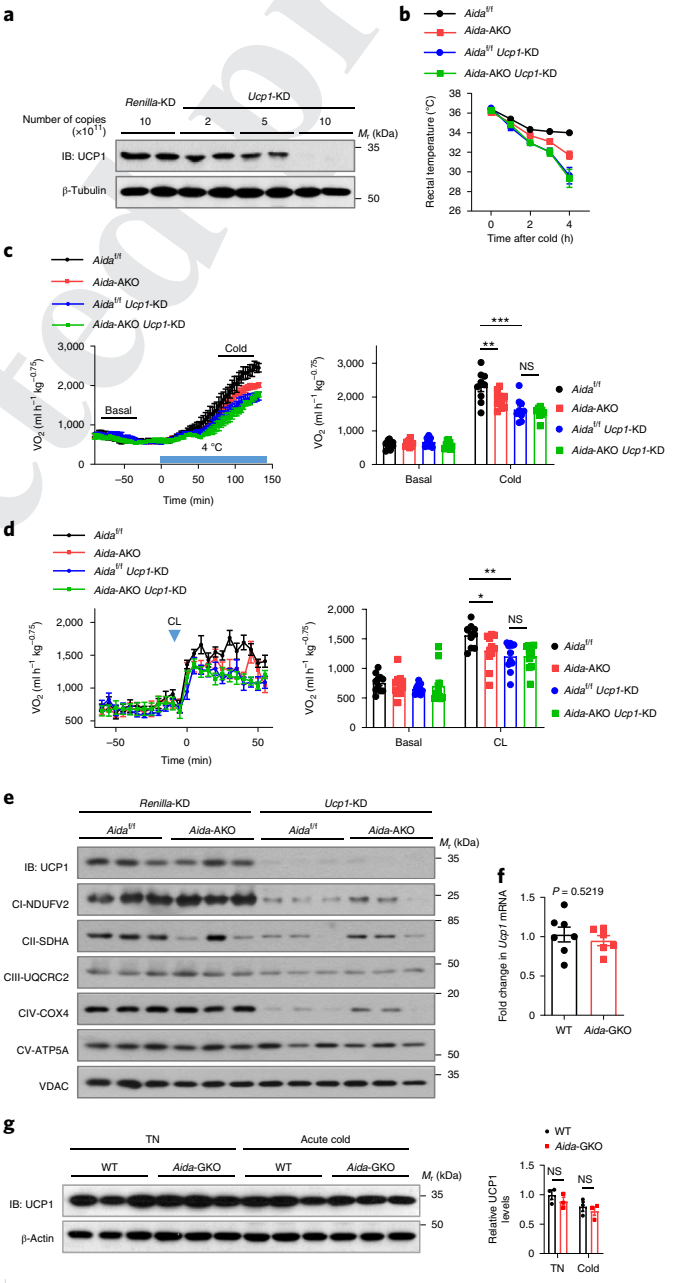

Fig. 4 | AIDA-mediated adaptive thermogenesis is dependent on UCP1. **a**, Knockdown efficiency of *Ucp1* in BAT; $n=2$ mice. **b**, CTT of *Aida*$^{f/f}$ and *Aida*-AKO mice with AAV-mediated expression of shRNA targeting *Ucp1* or *Renilla*, as a control. Data are the mean ± s.e.m.; $n=10$ mice per group, except for the *Aida*-AKO group, where $n=12$. *Aida*$^{f/f}$ versus *Aida*$^{f/f}$ *Ucp1*-KD, $^{***}P=0.0004$ (2 h), $^{**}P=0.0015$ (3 h) and $^{**}P=0.0021$ (4 h); *Aida*$^{f/f}$ versus *Aida*-AKO, $^{***}P=0.0007$ (3 h), $^{***}P=0.0008$ (4 h); two-way RM ANOVA with Geisser–Greenhouse's correction, followed by Tukey. **c**,**d**, OCR of mice in **b** under acute cold exposure (**c**; $n=9$ mice per group, except for the *Aida*-AKO group, where $n=11$) or i.p. injected with 1 mg kg^{-1} CL316243 (CL; $n=11$ mice per group; **d**). Data are the mean ± s.e.m. of values normalized to the body weight (kg$^{0.75}$; left) or individual values with the mean ± s.e.m. of the average OCR under basal and stressed conditions (right). **c**, The basal values were calculated as the average of 30–60 min before the shift in ambient temperature; the values under cold were calculated as the average of 100–130 min after the temperature shift. *Aida*$^{f/f}$ versus *Aida*-AKO, $^{**}P=0.0020$; *Aida*$^{f/f}$ versus *Aida*$^{f/f}$ *Ucp1*-KD, $^{***}P<0.0001$; *Aida*$^{f/f}$ *Ucp1*-KD versus *Aida*-AKO *Ucp1*-KD, $P=0.8047$; two-way RM ANOVA with Tukey. **d**, The basal-level and CL316243-stimulated values were calculated as the average values of 40 min before or after CL316243 injection, respectively. *Aida*$^{f/f}$ versus *Aida*-AKO, $^{*}P=0.0279$; *Aida*$^{f/f}$ versus *Aida*$^{f/f}$ *Ucp1*-KD, $^{**}P=0.0011$; *Aida*$^{f/f}$ *Ucp1*-KD versus *Aida*-AKO *Ucp1*-KD, $P>0.9999$; two-way RM ANOVA with Tukey. **e**, Mitochondrial complexes I–V (CI–CV) in BAT from mice after acute cold; $n=3$ mice. **f**, *Ucp1* mRNA in the BAT of mice after acute cold (6 h in 4 °C after fasting). Data are the mean ± s.e.m. *Aida*-GKO, $n=6$; and WT, $n=7$ mice. **g**, UCP1 in the BAT of mice before and after acute cold exposure. The levels of UCP1 relative to β-actin were quantified and are shown as the mean ± s.e.m. (right); $n=3$ mice; ordinary two-way ANOVA with Tukey. $^{*}P<0.05$; $^{**}P<0.005$; $^{***}P<0.05$; NS, not significant. Uncropped blots for **a**,**e**,**g** and numerical source data for **b**–**d**,**f**,**g** are provided.

Uncorrected proofs

oxidation is required for the AIDA-mediated activation of UCP1. Notably, depletion of ROS by NAC did not affect AIDA phosphorylation or the interaction between AIDA and UCP1 (Extended Data Fig. 8b,c). These results suggest that, despite both being dependent on PKA, cold-induced ROS production and the phosphorylation of AIDA are separate events downstream of adrenergic stimulation.

Fatty acids are known regulators of UCP1. We next explored the role of AIDA in the PKA-mediated lipolytic pathway. Deletion of *Aida* did not affect the increased levels of fatty acids generated from lipolysis in stimulated adipose tissues (Extended Data Fig. 9a). Consistent with these results, AIDA deficiency had no effect on the activational phosphorylation of HSL or the protein abundance of ATGL and HSL—two key lipases involved in lipolysis—under stimulation by forskolin (Extended Data Fig. 9b). Therefore, AIDA does not seem to have a role in adrenergic induction of lipid mobilization. However, AIDA deficiency still impairs adaptive thermogenesis both in vivo and in vitro, even when compared with mice or cells pretreated with an ATGL inhibitor (Extended Data Fig. 9c,d), thereby indicating that AIDA and fatty acids are two independent factors downstream of PKA that activate UCP1 synergistically. Collectively, our data demonstrate that AIDA plays a critical role in integrating the two parallel pathways of increased lipolysis and ROS-triggered UCP1 oxidative modification in acute stress responses (Extended Data Fig. 9e).

Discussion

Our study suggests a model in which AIDA receives sympathetic input as a direct substrate of PKA to stimulate the thermogenic activity of UCP1 via direct interaction (Extended Data Fig. 9e). In this process, PKA is a bifurcated node, stimulating lipolysis to boost energy production that causes elevated ROS levels and at the same time independently phosphorylating AIDA. Importantly, although we have provided data showing that PKA can directly phosphorylate AIDA (Fig. 3c), it cannot be ruled out that PKA could also lead to AIDA phosphorylation indirectly. Following phosphorylation by PKA, AIDA binds to UCP1 to facilitate ROS-dependent oxidative modification of UCP1, which ultimately promotes UCP1 activation. Whole-body or adipocyte-specific knockout of *Aida* impairs adaptive thermogenesis in BAT, leading to hypothermia following exposure to cold (Fig. 1a,c). The importance of PKA-mediated phosphorylation of AIDA at S161 is underscored by the observation that the reintroduction of a S161A mutant, unlike WT-AIDA, into *Aida*-GKO mice failed to rescue thermogenesis (Fig. 3e,f and Extended Data Fig. 5b). These findings establish a transcriptional activation-independent mechanism for the SNS to regulate UCP1 in the acute stress responses.

It is known that the SNS plays a pivotal role in BAT thermogenesis, muscle shivering as well as cutaneous vasoconstriction[33,34]. The function of AIDA seems to be primarily under the control of sympathetic innervation to BAT, as mice with AIDA depletion showed no further compromise in thermogenesis after surgical sympathetic denervation in interscapular BAT (iBAT; Fig. 2a,b and Extended Data Fig. 2a) or pretreated with β-adrenergic blockers (Fig. 2c and Extended Data Fig. 2b). Moreover, we confirmed that the effect of AIDA on thermogenesis is dependent on UCP1 (Fig. 4b,c). Notably, *Ucp1*-KD showed varied effects on electron-transport-chain proteins under acute cold stimulation (Fig. 4e), which seemed to be generally milder than that observed in cold-acclimated mice genetically lacking *Ucp1* (ref. [35]). Importantly, the adipose-specific knockout of *Aida* alone had no apparent effect on the electron-transport-chain proteins (Fig. 4e), implying that AIDA may specifically regulate the uncoupling activity of UCP1 under acute cold conditions but does not affect the overall role of UCP1 in mitochondrial homeostasis.

It is important to note that AIDA acts to instigate UCP1 thermogenesis without affecting the upstream steps, including sympathetic innervation of BAT and the adrenergic signalling cascade. Several important peripheral signals converge on common energy sensors, such as AMP-activated protein kinase, to modulate sympathetic tone on BAT[36,37]. However, alteration of these factors, if any due to AIDA deficiency, may not be a significant contributor to the deficiency in the regulation of body temperature in *Aida*-KO mice. *Aida*-KO brown adipocytes have intact intracellular signalling, which can be seen from the unchanged levels of lipolytic enzymes and mobilized fatty acids (Extended Data Fig. 9a,b). The increase in ROS in brown adipocytes after adrenergic stimulation is also independent of AIDA. On the other hand, PKA phosphorylates AIDA to cause its binding to UCP1, which may in turn undergo certain conformational changes and render the cysteine of UCP1 more accessible to oxidation[21].

It is noteworthy that although ATGL inhibition already significantly impairs UCP1 activity, AIDA deficiency causes a more severe impairment of UCP1 activity (Extended Data Fig. 9c,d). This indicates that the effect of AIDA in thermogenesis could be divided into fatty acid-dependent and -independent parts, suggesting that AIDA acts as an integrator of the various effects of adrenergic signalling, including lipolysis and generation of ROS. We indeed found that NAC totally blocked AIDA-dependent adaptive thermogenesis (Fig. 6e,f and Extended Data Fig. 8a), indicating that AIDA is involved in ROS-mediated thermogenesis. Consistent with our finding, recent studies have shown that circulating succinate and BCAA contribute to UCP1-dependent thermogenesis in BAT by

Fig. 5 | AIDA interacts with UCP1. a, UCP1 interacts with AIDA in HEK293T cells after forskolin (10 μM) stimulation. **b**, Co-immunoprecipitation of endogenously expressed AIDA and UCP1 using BAT from WT mice that were unstressed or exposed to cold for 3 h. **a**,**b**, The intensities of immunoprecipitated AIDA relative to immunoprecipitated UCP1 were standardized among three independent experiments and are shown as the mean ± s.e.m. (bottom). Two-tailed unpaired Student's *t*-test. **c**, Design of the assay for analysing AIDA-associated organelles. Several elements of this image were modified from images from Servier Medical Art by Servier (https://smart.servier.com/) licensed under a Creative Commons Attribution 3.0 Unported License (https://creativecommons.org/licenses/by/3.0/). **d**,**e**, Analysis of AIDA-associated organelles. AAV carrying HA–AIDA, HA–S161A-AIDA or AAV vector was delivered into mice via the tail vein. Four weeks after the viral administration, the mice were fasted overnight and kept in individual cages at 23 °C or 4 °C for 3 h. Next, BAT was isolated and homogenized for detergent-free IP using anti-HA magnetic beads. Quantification of the relative intensities of AIDA, VDAC, TOM20 and TIM23 in the immunoprecipitates was standardized among three independent experiments and are shown as the mean ± s.e.m. (right). Ordinary two-way ANOVA with Tukey. **f**, Electron microscopy analysis of the localization of APEX2-tagged WT-AIDA or S161A-AIDA in BAT from mice fasted overnight and kept in individual cages at 4 °C for 3 h. The electron-dense staining along the mitochondrial cristae indicates the location of AIDA. Scale bar, 0.1 μm. Images are representative of two independent experiments with similar results. Magnified views of the boxed regions in the main images are shown (right). **g**, Forskolin did not promote an interaction between S161A-AIDA and UCP1. HEK293T cells were transfected with HA-tagged WT-AIDA or S161A-AIDA together with FLAG-tagged UCP1. Following 1 h of treatment with forskolin (10 μM), the cells were lysed and subjected to immunoprecipitation against HA. Phosphorylation (p-) of AIDA was determined using a phospho-site-specific antibody. The intensities of the immunoprecipitated UCP1 and p-S161-AIDA relative to AIDA were standardized among three independent experiments and are shown as the mean ± s.e.m. (right). Ordinary two-way ANOVA with Tukey. IB, immunoblot; IP, immunoprecipitation; CoIP, co-immunoprecipitation; RT, room temperature; TCL, total cell lysate. **a**,**b**,**d**,**e**,**g**, Uncropped blots and numerical source data are provided.

Uncorrected Proofs

increasing ROS[38,39], suggesting that there exist at least two distinct UCP1 activation routes that are directly triggered by either fatty acids or ROS. It is possible that under severe stress, such as cold, these factors are required in concert for optimal activation of UCP1, whereas milder stimulations could count on single mechanisms. In summary, our findings have elucidated a regulatory mechanism for UCP1 thermogenic activity in response to acute cold stress. We have provided a model that AIDA, as a direct substrate of PKA activated

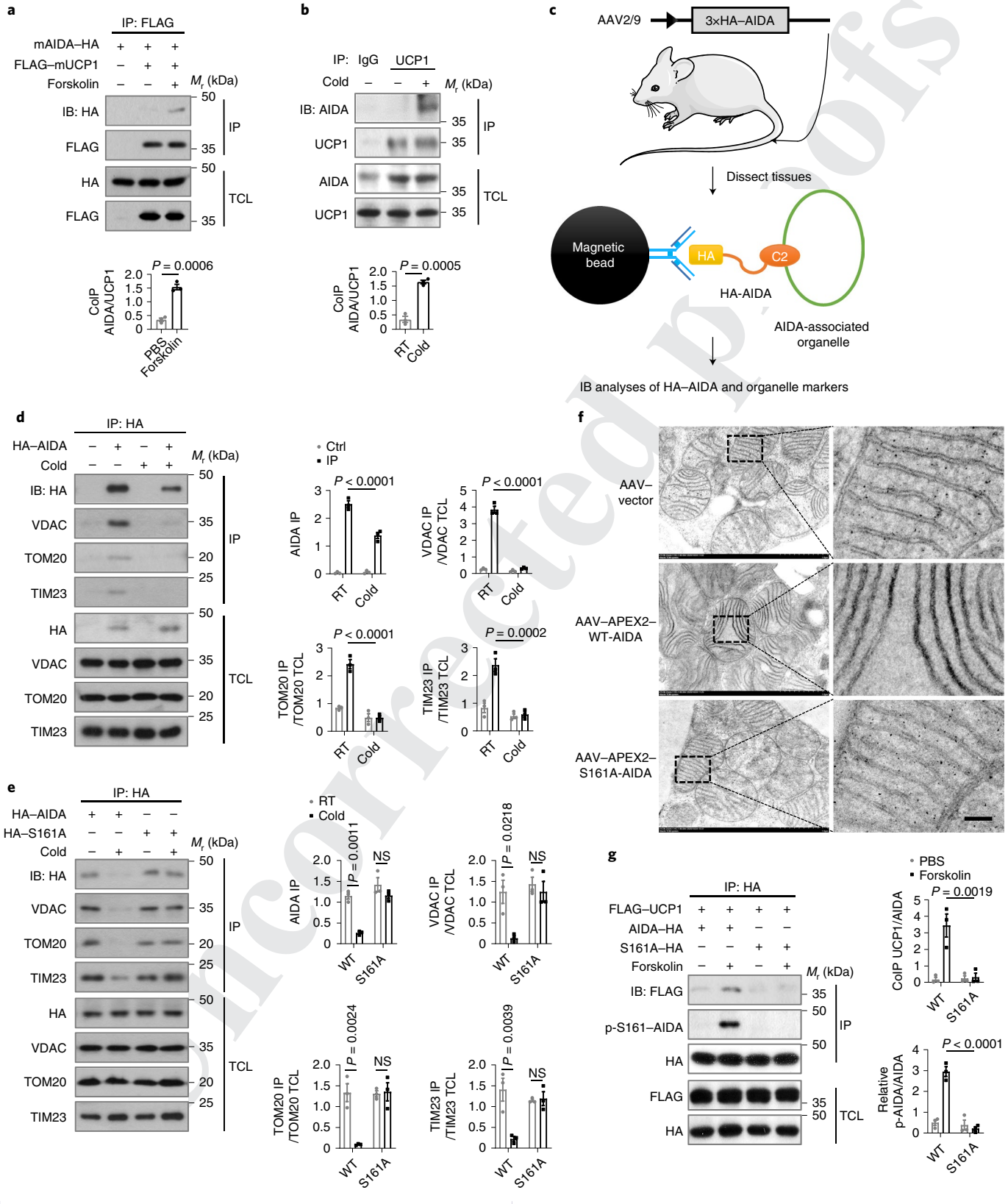

Uncorrected Proofs

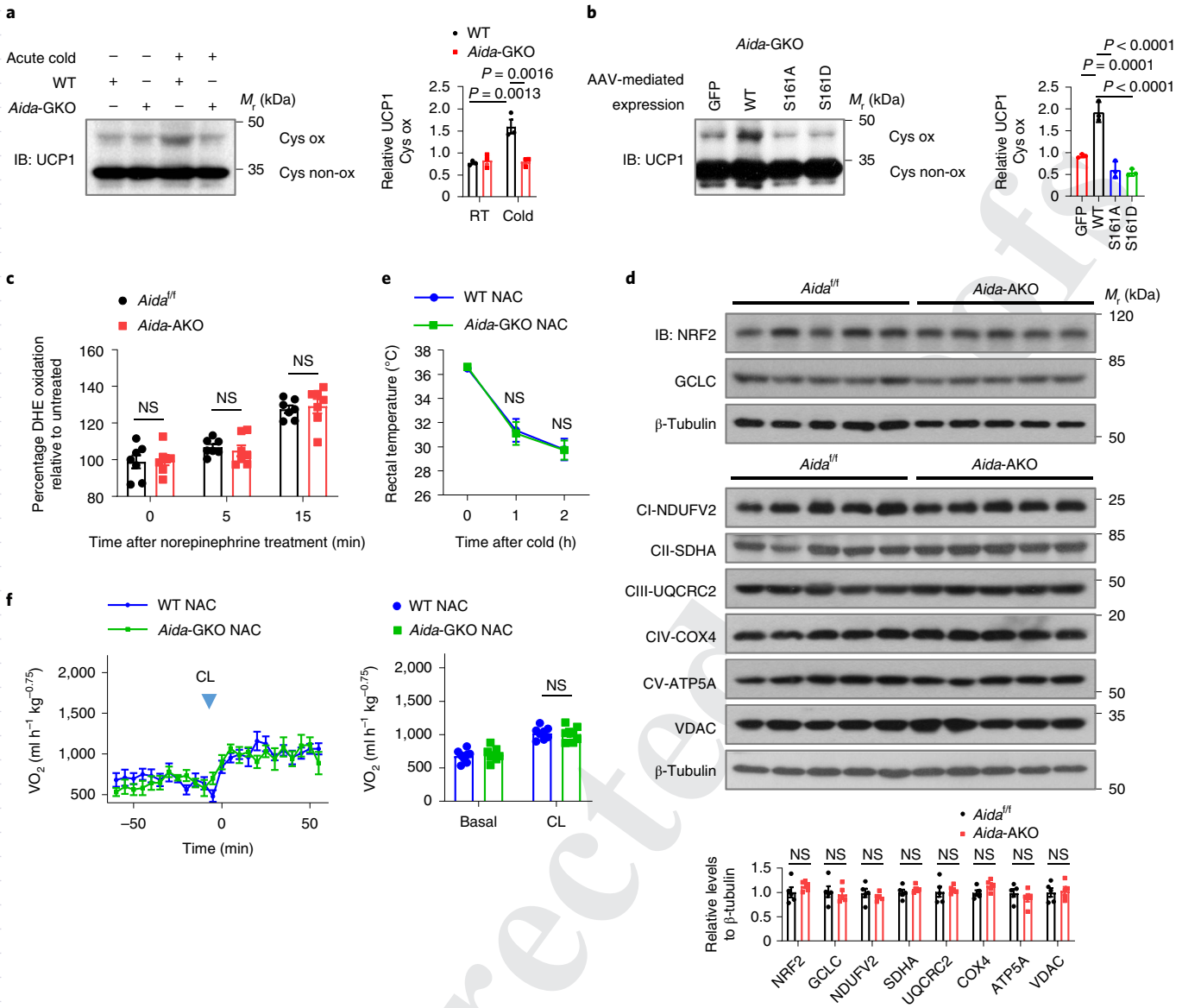

Fig. 6 | AIDA enhances the oxidative modification of UCP1. a,**b**, Immunoblotting analysis of the oxidative modification of UCP1 in mice exposed to cold. Brown adipose tissue from WT and *Aida*-GKO mice (**a**), and *Aida*-GKO mice re-expressing different AIDA constructs and GFP, as a control, in BAT (**b**) exposed to 4 °C for 3 h were homogenized and incubated with polyethylene glycol maleimide, followed by immunoblot analysis. Cys ox, oxidatively modified UCP1; Cys non-ox, unmodified UCP1; RT, room temperature. The relative intensities of oxidatively modified UCP1 were standardized among three independent experiments and are shown as the mean ± s.e.m. (right). Ordinary two-way ANOVA with Tukey (**a**) or Dunnett (**b**). **c**, Levels of ROS in brown adipocytes treated with norepinephrine. The production of ROS was detected by oxidation of dihydroethidium (DHE) and ratiometric assessment. Data are the individual values with the mean ± s.e.m. from the brown adipocytes of $n = 7$ mice per group. Two-way RM ANOVA with Geisser–Greenhouse's correction, followed by Sidak. **d**, Protein abundance of antioxidative regulators and mitochondrial proteins in BAT from mice after acute cold stimulation. The protein levels relative to β-tubulin are shown as the mean ± s.e.m. (bottom). CI–CV, mitochondrial complexes I–V; two-tailed unpaired Student's *t*-test; $n = 5$ mice. **e**, CTT of mice pretreated with NAC. Female WT and *Aida*-GKO mice were i.p. injected with NAC (500 mg kg^{-1}) 10 min before cold exposure. Data are the mean ± s.e.m.; $n = 7$ mice per group. $P = 0.9961$ (1 h) and, $P > 0.9999$ (2 h); two-way RM ANOVA with Geisser–Greenhouse's correction, followed by Sidak. **f**, OCR of mice before and after CL316243 injection with NAC pretreatment. The mice (WT and *Aida*-GKO) were i.p. injected with NAC (500 mg kg^{-1}) 10 min before injection with CL316243 (CL; 1 mg kg^{-1}). Data were collected from $n = 8$ mice per group and are expressed as the mean ± s.e.m. of the values normalized to the body weight (kg$^{0.75}$; left) or individual values with the mean ± s.e.m. of the average OCR before and after the CL316243 injection (right). $P = 0.9633$; two-way RM ANOVA with Sidak. NS, not significant; IB, immunoblot. Uncropped blots for **a**,**b**,**d** and numerical source data for **a**–**f** are provided.

by the adrenergic signalling from the SNS route, acts to converge the induction of lipolysis and increased ROS production to oxidation of UCP1, thereby instigating robust thermogenesis in response to acute cold stress (Extended Data Fig. 9e).

Online content

Any methods, additional references, Nature Research reporting summaries, source data, extended data, supplementary information, acknowledgements, peer review information; details of

Uncorrected

author contributions and competing interests; and statements of data and code availability are available at https://doi.org/10.1038/s41556-021-00642-9.

Received: 10 February 2020; Accepted: 28 January 2021;

References

1. Cannon, B. & Nedergaard, J. Brown adipose tissue: function and physiological significance. *Physiol. Rev.* **84**, 277–359 (2004).
2. Kajimura, S. & Saito, M. A new era in brown adipose tissue biology: molecular control of brown fat development and energy homeostasis. *Annu Rev. Physiol.* **76**, 225–249 (2014).
3. Chouchani, E. T. & Kajimura, S. Metabolic adaptation and maladaptation in adipose tissue. *Nat. Metab.* **1**, 189–200 (2019).
4. Chouchani, E. T., Kazak, L. & Spiegelman, B. M. New advances in adaptive thermogenesis: UCP1 and beyond. *Cell Metab.* **29**, 27–37 (2019).
5. Ballinger, M. A. & Andrews, M. T. Nature's fat-burning machine: brown adipose tissue in a hibernating mammal. *J. Exp. Biol.* **221**, jeb162586 (2018).
6. Enerback, S. et al. Mice lacking mitochondrial uncoupling protein are cold-sensitive but not obese. *Nature* **387**, 90–94 (1997).
7. Shabalina, I. G. et al. Cold tolerance of UCP1-ablated mice: a skeletal muscle mitochondria switch toward lipid oxidation with marked UCP3 up-regulation not associated with increased basal, fatty acid- or ROS-induced uncoupling or enhanced GDP effects. *Biochim. Biophys. Acta* **1797**, 968–980 (2010).
8. Keipert, S. et al. Long-term cold adaptation does not require FGF21 or UCP1. *Cell Metab.* **26**, 437–446 (2017).
9. Ortega, S. P., Chouchani, E. T. & Boudina, S. Stress turns on the heat: regulation of mitochondrial biogenesis and UCP1 by ROS in adipocytes. *Adipocyte* **6**, 56–61 (2017).
10. Tank, A. W. & Lee Wong, D. Peripheral and central effects of circulating catecholamines. *Compr. Physiol.* **5**, 1–15 (2015).
11. Bartness, T. J., Vaughan, C. H. & Song, C. K. Sympathetic and sensory innervation of brown adipose tissue. *Int J. Obes.* **34**, S36–S42 (2010).
12. Vaughan, C. H., Zarebidaki, E., Ehlen, J. C. & Bartness, T. J. Analysis and measurement of the sympathetic and sensory innervation of white and brown adipose tissue. *Methods Enzymol.* **537**, 199–225 (2014).
13. Zeng, X. et al. Innervation of thermogenic adipose tissue via a calsyntenin 3β–S100b axis. *Nature* **569**, 229–235 (2019).
14. Cao, W., Medvedev, A. V., Daniel, K. W. & Collins, S. β-Adrenergic activation of p38 MAP kinase in adipocytes: cAMP induction of the uncoupling protein 1 (UCP1) gene requires p38 MAP kinase. *J. Biol. Chem.* **276**, 27077–27082 (2001).
15. Puigserver, P. et al. A cold-inducible coactivator of nuclear receptors linked to adaptive thermogenesis. *Cell* **92**, 829–839 (1998).
16. Fedorenko, A., Lishko, P. V. & Kirichok, Y. Mechanism of fatty-acid-dependent UCP1 uncoupling in brown fat mitochondria. *Cell* **151**, 400–413 (2012).
17. Jastroch, M., Hirschberg, V. & Klingenspor, M. Functional characterization of UCP1 in mammalian HEK293 cells excludes mitochondrial uncoupling artefacts and reveals no contribution to basal proton leak. *Biochim. Biophys. Acta* **1817**, 1660–1670 (2012).
18. Zhao, L. et al. Specific interaction of the human mitochondrial uncoupling protein 1 with free long-chain fatty acid. *Structure* **25**, 1371–1379 (2017).
19. Crichton, P. G., Lee, Y. & Kunji, E. R. The molecular features of uncoupling protein 1 support a conventional mitochondrial carrier-like mechanism. *Biochimie* **134**, 35–50 (2017).
20. Woyda-Ploszczyca, A. M. & Jarmuszkiewicz, W. The conserved regulation of mitochondrial uncoupling proteins: from unicellular eukaryotes to mammals. *Biochim. Biophys. Acta Bioenerg.* **1858**, 21–33 (2017).
21. Chouchani, E. T. et al. Mitochondrial ROS regulate thermogenic energy expenditure and sulfenylation of UCP1. *Nature* **532**, 112–116 (2016).
22. Sebaa, R. et al. SIRT3 controls brown fat thermogenesis by deacetylation regulation of pathways upstream of UCP1. *Mol. Metab.* **25**, 35–49 (2019).
23. Wang, G. et al. Regulation of UCP1 and mitochondrial metabolism in brown adipose tissue by reversible Succinylation. *Mol. Cell* **74**, 844–857 (2019).
24. Luo, H. et al. AIDA selectively mediates downregulation of fat synthesis enzymes by ERAD to retard intestinal fat absorption and prevent obesity. *Cell Metab.* **27**, 843–853 (2018).
25. Zheng, L. S. et al. Structure and mechanism of the unique C2 domain of Aida. *FEBS J.* **281**, 4622–4632 (2014).
26. Crane, J. D., Mottillo, E. P., Farncombe, T. H., Morrison, K. M. & Steinberg, G. R. A standardized infrared imaging technique that specifically detects UCP1-mediated thermogenesis in vivo. *Mol. Metab.* **3**, 490–494 (2014).
27. Jimenez, V. et al. In vivo adeno-associated viral vector-mediated genetic engineering of white and brown adipose tissue in adult mice. *Diabetes* **62**, 4012–4022 (2013).
28. Cassard-Doulcier, A. M., Gelly, C., Bouillaud, F. & Ricquier, D. A 211-bp enhancer of the rat uncoupling protein-1 (UCP-1) gene controls specific and regulated expression in brown adipose tissue. *Biochem. J.* **333**, 243–246 (1998).
29. Larose, M. et al. Essential *cis*-acting elements in rat uncoupling protein gene are in an enhancer containing a complex retinoic acid response domain. *J. Biol. Chem.* **271**, 31533–31542 (1996).
30. Zhou, Z. et al. Endoplasmic reticulum-associated degradation regulates mitochondrial dynamics in brown adipocytes. *Science* **368**, 54–60 (2020).
31. Martell, J. D., Deerinck, T. J., Lam, S. S., Ellisman, M. H. & Ting, A. Y. Electron microscopy using the genetically encoded APEX2 tag in cultured mammalian cells. *Nat. Protoc.* **12**, 1792–1816 (2017).
32. Requejo, R. et al. Measuring mitochondrial protein thiol redox state. *Methods Enzymol.* **474**, 123–147 (2010).
33. Hensel, H. Neural processes in thermoregulation. *Physiol. Rev.* **53**, 948–1017 (1973).
34. Silva, J. E. Thermogenic mechanisms and their hormonal regulation. *Physiol. Rev.* **86**, 435–464 (2006).
35. Kazak, L. et al. UCP1 deficiency causes brown fat respiratory chain depletion and sensitizes mitochondria to calcium overload-induced dysfunction. *Proc. Natl Acad. Sci. USA* **114**, 7981–7986 (2017).
36. Lage, R., Ferno, J., Nogueiras, R., Dieguez, C. & Lopez, M. Contribution of adaptive thermogenesis to the hypothalamic regulation of energy balance. *Biochem. J.* **473**, 4063–4082 (2016).
37. Contreras, C., Nogueiras, R., Dieguez, C., Rahmouni, K. & Lopez, M. Traveling from the hypothalamus to the adipose tissue: the thermogenic pathway. *Redox Biol.* **12**, 854–863 (2017).
38. Mills, E. L. et al. Accumulation of succinate controls activation of adipose tissue thermogenesis. *Nature* **560**, 102–106 (2018).
39. Yoneshiro, T. et al. BCAA catabolism in brown fat controls energy homeostasis through SLC25A44. *Nature* **572**, 614–619 (2019).

Publisher's note Springer Nature remains neutral with regard to jurisdictional claims in published maps and institutional affiliations.

© The Author(s), under exclusive licence to Springer Nature Limited 2021

Uncorrected Proofs

Methods

Mice. Male mice with ad libitum access to regular chow diet and water were maintained at 22–24 °C with 55–60% humidity and a 12 h light–12 h dark cycle, unless otherwise indicated in the figure legends. The nesting materials in the cages were changed once a week. All of the mice were in a C57BL/6 background. Mice were used for primary culture of brown and white adipocytes as well as AAV injection at the age of 6 weeks. Adult mice (aged 12–18 weeks) were used for the in vivo experiments (CTT, indirect calorimetry, infrared thermography and so on). Experiments were performed with sex- and age-matched *Aida*-knockout and control littermate mice. *Aida*$^{f/f}$ mice and *Aida*-GKO mice were generated as described previously[24]. The *Aida*$^{f/f}$ mice were bred with *Adipoq–cre* or *Ucp1–cre* mice to obtain *Aida*-AKO mice or *Aida*-BKO mice, respectively. The primers that were used for genotyping are listed in Supplementary Table 1. All animal studies were approved by the Institutional Animal Care and Use Committee at Xiamen University.

Primary adipocyte culture. Following dissection from six-week-old mice and rinsing in ice-cold PBS, the adipose tissues were minced and incubated in a digestion buffer (2% essentially fatty acid-free BSA and 1.5 mg ml^{-1} collagenase IV in 1× HBSS) for 1 h at 37 °C. The tissue suspension was then filtered through a 100-μm cell strainer and centrifuged at 700*g* for 10 min to pellet the stromal vascular fibroblasts. The stromal vascular fibroblasts were cultured in a DMEM/F12 1:1 medium with 10% fetal bovine serum (FBS) until confluency was reached. The cells were next differentiated into mature adipocytes. Specifically, for brown adipocytes, the cells were cultured in an induction medium (DMEM/F12 1:1 medium with 10% FBS containing 5 μg ml^{-1} insulin, 1 nM 3,3′,5-triiodo-L-thyronine, 125 μM indomethacin, 0.5 mM isobutylmethylxanthine and 1 μM dexamethasone) for 2 d. The medium was then changed to a maintenance medium (DMEM/F12 1:1 medium with 10% FBS supplemented with 5 μg ml^{-1} insulin and 1 nM 3,3′,5-triiodo-L-thyronine) for another 6 d. For white adipocytes, the cells were cultured in an induction medium (DMEM/F12 1:1 medium with 10% FBS containing 5 μg ml^{-1} insulin, 0.5 mM isobutylmethylxanthine and 1 μM dexamethasone) for 2 d. The medium was then changed to a maintenance medium (DMEM/F12 1:1 medium with 10% FBS supplemented with 5 μg ml^{-1} insulin) for another 6 d. The medium was replaced with fresh maintenance medium every other day.

Plasmid construction. The complementary DNA templates for marmot, hedgehog and hamster *Aida* as well as *Ucp1* were obtained from reverse-transcribed RNA extracted from BAT of the respective animals. *Aida* and *Prkaca* from *B. floridae* were cloned using a reverse-transcribed RNA extracted from *B. floridae* of mixed developmental stages. Primers binding to the highly conserved regions were designed from the available NCBI sequences (*Erinaceus europaeus AIDA*, XM_007521310; *E. europaeus UCP1*, XM_007536316; *Mesocricetus auratus Aida*, XM_005078218; *M. auratus Ucp1*, NM_001281332; *Marmota marmota Aida*, XM_015483616; *M. marmota Ucp1*, XM_015483616; *B. floridae Aida*, XM_002613256; and *B. floridae cAMP-dependent protein kinase*, XM_002600401.1). The cloned cDNAs were sequenced and deposited in the GenBank database (accession numbers: MT114182, *B. floridae Aida*; MT114183, *E. europaeus Ucp1*; MT114184, *M. auratus Ucp1*, MT114185, *M. auratus Aida*; MT114186, *Marmota himalayana Ucp1*; MT114187, *B. floridae Prkaca*; MT759803, *M. himalayana Aida*; and MT759804, *E. europaeus Aida*). The HA-tagged mouse S161A-AIDA and S161D-AIDA or *B. floridae* P163S-AIDA in pcDNA3.3 were cloned by PCR-based site-directed mutagenesis using PrimeSTAR DNA polymerase (Takara Bio-tech Co. Ltd).

AAV. The plasmids for the AAV2/9 system were used for the KD or overexpression of genes in vivo. This system contains a transgene plasmid with a promoter and target cDNA or short hairpin RNA placed between the two 145-base *ITR*s (from type 2 AAV), a transfer plasmid with sequences coding for REP (from type 2 AAV) and CAP (from type 9 AAV), and a helper plasmid with E4, E2a and VA (from adenovirus). The transgene plasmids carry the *CMV* promoter for global expression of genes, the mini-promoter and enhancer of *Ucp1* for BAT-specific expression of genes[28] and the m*U6* promoter for the KD experiments. The plasmids were mixed and transfected into HEK293T cells. The cells and the medium containing packaged viruses were collected 60–72 h after transfection. The cells were then lysed through three rounds of freezing in liquid nitrogen, followed by thawing in a 37 °C incubator. Next, 5×polyethylene glycol (PEG; 40% PEG-8000, 2.5 M NaCl) was added to the medium to a final concentration of 8% PEG-8000 and 0.5 M NaCl and incubated overnight at 4 °C. After centrifugation, the cell lysates and the PEG pellet were mixed. The mixture was purified in 17, 25, 40 and 60% iodixanol (Sigma-Aldrich) gradients by ultracentrifugation. The viruses were extracted from the 40% iodixanol gradient and washed three times with PBS in ultrafiltration tubes through centrifugation. The copy numbers of AAV were determined by quantitative PCR (Bio-Rad, CFX96); the primers that were used are listed in Supplementary Table 2. AAV for KD (1×10^{12} copies per mouse) or overexpression (0.4×10^{12} copies per mouse) were injected into the tail vein of six-week-old mice. After 3–4 weeks, the mice were killed to examine the efficiency of AAV.

Immunofluorescence staining. Primary brown adipocytes were incubated with virus supernatants containing polybrene (10 μg ml^{-1}) to express AIDA–HA at day 3 during differentiation. At 24 h after infection, the medium was replaced with fresh maintenance medium. At day 7 of differentiation, immunofluorescence staining was performed as previously described[24]. For detailed antibody information, see Supplementary Table 3.

CTT. Before the test, the mice were starved overnight and then moved to individual cages at 4 °C without food or water. The rectal temperature was measured using a thermal probe pretreated with Vaseline and a type K digital thermometer (EXTECH, model 421501).

Indirect calorimetry. The mice were housed individually in metabolic chambers for 4 d to minimize the stress of housing change. The mice were then measured in the calorimetry chambers for another 2 d with a high-resolution recording at 5-min intervals (Sable Systems International, CAB-16-1-EU). For CL316243 treatment, the basal metabolic rates of the mice kept at thermoneutrality (30 °C) were measured for 3–4 h. Next, the mice were i.p. injected with CL316243 (1 mg kg^{-1}) and measured in the calorimetry chambers with recordings at 5-min intervals at thermoneutrality (Sable Systems International, CAB-16-1-EU). For the experiment with acute cold stimulation, mice that had been preconditioned to thermoneutrality (30 °C) were starved overnight. The temperature was changed to 4 °C during a high-resolution recording at 3-min intervals (TSE Systems Phenomaster, ESCE-16).

Body-composition analysis. The fat and lean mass of the mice were analysed using a 3-in-1 Echo MRI composition analyser (Echo Medical Systems, 100H).

Gene expression analysis. RNA was extracted from frozen tissues using TRIzol, followed by a PureLink RNA mini kit (Thermo Fisher Scientific Inc.). Reverse transcription was performed on 1 μg purified RNA using a High-capacity cDNA reverse transcription kit (Toyobo Co., Ltd). Real-time quantitative PCR was performed using SYBR Green probes (AB STEP PLUS ONE, Applied Biosystems). The expression levels of *Ucp1* are presented as normalized fold changes to the geographical mean of the mRNA abundance of *Ppia* and *Tbp1* using the comparative C_t method. The primers that were used are listed in Supplementary Table 2.

Respiration assays. Primary adipocytes were cultured and differentiated in XF96 microplates. At day 7 of differentiation, the cells were washed once and incubated in a pre-warmed assay medium (XF basal medium supplemented with 25 mM glucose, 2 mM GlutaMax and 2% fatty acid-free BSA, pH 7.4) at 37 °C in a room-air incubator for 1 h. The drug-injection ports of the sensor cartridges were loaded with the assay reagents at 10× in assay medium (without BSA). The respiration rates of the brown adipocytes were measured for three cycles for basal respiration, three cycles for oligomycin (5 μM) treatment, six cycles for ISO-stimulated respiration, three cycles for maximum respiration after addition of FCCP treatment (1 μM), and three cycles for non-mitochondrial respiration with the addition of rotenone (2.5 μM) and antimycin-A (5 μM). Each cycle consisted of mixing for 3 min, waiting for 0 min and measurement for 3 min. The ISO-induced mitochondrial uncoupled respiration was calculated as the change in the ISO-induced mitochondrial uncoupling respiration rate over the basal mitochondrial uncoupling respiration rate. The OCR values were automatically calculated by the Seahorse XF96 software (Wave, Seahorse Bioscience).

Surgical denervation. The mice were anaesthetized with 1% sodium pentobarbital and the fur of the target area was removed. The area was wiped with povidone-iodine and a midline incision was made in the skin along the upper dorsal surface to expose both iBAT pads[12]. The iBAT was gently removed with tweezers to expose the lateral and ventral surfaces of the iBAT. Nerves are found in bundles of four or five just beneath the iBAT on each side of the iBAT. The nerves on both sides were cut in two locations and the cut sections were removed. The two lobes of the iBAT were then placed back in position and rinsed with saline. The incision in the skin was closed with wound clips and nitrofurazone powder was applied to the surface of the wound. The mice were kept at 37 °C until they woke up. The sham surgery of the control mice was performed as per the denervation surgery, except that the nerved were not cut or removed. The mice were allowed to recover from surgery for 2 weeks before data collection.

Analysis of AIDA-associated organelles. AAV vector or AAV carrying HA–WT-AIDA or HA–S161A-AIDA was delivered into the mice via the tail vein. Approximately 4 weeks after viral administration, the mice were fasted overnight and kept in individual cages at 4 °C or 23 °C for 3 h. Brown adipose tissue was then isolated from the euthanized mice and washed once with ice-cold PBS. Next, the BAT was cut into small pieces using scissors in KPBS (136 mM KCl and 10 mM KH_2PO_4, pH 7.25) containing proteasome- and phosphatase-inhibitor cocktails, and homogenized with a Teflon Potter–Elvehjem homogenizer. The homogenate was transferred into a centrifugation tube and centrifuged at 740*g* for 10 min at 4 °C. The supernatant was collected and centrifuged again at 740*g* for 10 min at

4 °C. A portion of the supernatant was collected as the total input. The remaining supernatant was subjected to immunoprecipitation with anti-HA magnetic beads (sc-500773, Santa Cruz Biotechnology) in KPBS for 3 h at 4 °C. The beads were then washed four times with T-BST (2% Tween 20) containing proteasome- and phosphatase-inhibitor cocktails. The final immunoprecipitates were then solubilized with SDS sample buffer and analysed by western blotting.

APEX2 electron microscopy imaging. APEX2 imaging was performed as previously described[31], with modifications. Mice with AAV-mediated expression of APEX2–WT-AIDA or APEX2–S161A-AIDA were fasted overnight and kept in individual cages at 4 °C for 3 h. The mice were then euthanized and the iBAT was immediately removed and immersed in a pre-cooled fixation buffer (2.5% glutaraldehyde, 0.1 M phosphate buffer (PB), pH 7.4) cut into blocks of 2×2×2 mm. These blocks were further fixed for 6 h at 4 °C and kept overnight in 1/3 pre-cold fixation buffer diluted with 0.1 M PB (0.1 M Na_2HPO_4/0.1 M NaH_2PO_4 ratio of 81:19). These blocks were then incubated in 20 mM glycine in PB for 10 min, washed in PB, incubated in a DAB–H_2O_2 solution (0.5 mg ml^{-1} DAB and 10 mM H_2O_2 in 0.1 M cold PB) for 1.5 h and post-fixed in OsO_4 (1% OsO_4 in PB) for 1 h at 4 °C. The blocks were then washed with double-distilled water and stained with uranyl acetate (2% uranyl acetate in double-distilled water) for 20 h at 4 °C in the dark. The blocks were then washed with double-distilled water, followed by serial dehydration in 20, 50, 70, 90 and 100% ethanol at 4 °C and then 100% ethanol at room temperature, each for 15 min. After embedding in Spurr's resin/ethanol mixture (1:1 vol/vol) for 45 min, the pure Spurr's resin was added to the blocks. The pure Spurr's resin was replaced every 90 min (three times) and the blocks were placed in a 70 °C oven for 24 h. The blocks were then sectioned into 75-nm slices and images were taken using an electron microscope (Hitachi, HT-7800).

Immunoprecipitation. Proteins were extracted from homogenized BAT or cultured cells in RIPA buffer (20 mM Tris–HCl, pH 7.5, 150 mM NaCl, 1 mM EDTA, 1 mM EGTA, 1% NP-40, 1% sodium deoxycholate, proteasome- and phosphatase-inhibitor cocktails) and subjected to immunoprecipitation using different tagged beads, as specified in the figure legends, for 2–3 h at 4 °C. For detailed antibody information, see Supplementary Table 3.

Immunoblotting. Immunoblotting was performed as described previously[24]. Briefly, the cells or tissues were lysed in RIPA buffer and the cell or tissue extracts were mixed with SDS sample buffer. The samples were heated in boiled water for 5 min and subjected to SDS–PAGE and electrophoretic transfer. For experiments using Phos-tag gel, $MnCl_2$ (100 µM) and Phos-tag acrylamide AAL-107 (10 µM; FUJIFILM Wako Diagnostics USA Corporation) were added to the lower gel and manganese ions in the gel were chelated by EDTA (1 mM) before electrophoretic transfer. For detailed antibody information, see Supplementary Table 3.

Long-term cold adaptation. The mice were first transferred from 24 °C to 18 °C and allowed to adapt for 1 week. The mice were then transferred from 18 °C to 4 °C and maintained at 4 °C for another 4 weeks. The mice were single housed with free access to food and water throughout the process of cold adaptation.

Serum analysis. Blood was obtained from the eyeballs of the mice and clotted at room temperature for 1 h. The samples were then centrifuged (10 min, 1,500*g*, 4 °C) and the supernatants were collected and stored at −80 °C until use. Commercial assay kits were used following the manufacturer's instructions. A microplate reader (BMG LABTECH GmBH, Omega POLARstar) was used to collect the data. Concentrations were calculated using standard curves with specific dilution ratios of serum.

Infrared thermography. *Aida*-GKO mice were anaesthetized with 2% sodium pentobarbital, followed by i.p. injection of PBS or CL316243 (1 mg kg^{-1}). The anaesthetized mice were placed on a homothermic pad kept at 37 °C. The mice were subjected to infrared imaging 1 h post stimulation, and the temperature of their interscapular areas was determined using an infrared imaging device (Junctec, Ax5)[26].

Subcellular fractionation. The whole BAT from mice injected with PBS or CL316243 (1 mg kg^{-1}) was dissected and homogenized with a Teflon Potter Elvehjem homogenizer in a buffer containing 50 mM Tris–HCl, pH 7.4, 50 mM NaF, 1 mM EDTA and 0.25 M sucrose with proteasome- and phosphatase-inhibitor cocktails. A portion of the homogenate was saved as the total input. The remaining homogenate was centrifuged at 170,000*g* for 1 h. The supernatant was collected as the cytosol fraction and the pellet was collected as the total membrane fraction. The total membrane was further separated through centrifugation at 3,000*g* for 10 min, 15,000*g* for 10 min and 170,000*g* for 1 h. Each fraction was mixed with SDS sample buffer and analysed by immunoblotting.

In vitro kinase assay. Myc-tagged PRKACA was overexpressed in HEK293T cells and immunoprecipitated with Myc-tag antibody-coupled beads in RIPA buffer. The immunoprecipitates were washed three times each with RIPA buffer and kinase reaction buffer (50 mM Tris–HCl, pH 7.4, 50 mM NaCl and 2 mM $MgCl_2$). The immunoprecipitated kinases were then incubated with 1 µg of bacterially expressed His-tagged AIDA in kinase reaction buffer supplemented with 200 µM ATP at 30 °C for 20 min. Each sample was mixed with SDS sample buffer and analysed by immunoblotting.

Assessment of UCP1 thiol redox state. The mice were preconditioned at thermoneutrality for 3 d. After acute cold exposure at 4 °C for 3 h in individual cages without food and water, BAT from these mice were rapidly excised and homogenized with a Teflon Potter Elvehjem homogenizer in SHE buffer (250 mM sucrose, 5 mM HEPES, 1 mM EGTA and 1–2% fatty acid-free BSA) with the addition of 100 mM NEM and cocktails of proteasome and phosphatase inhibitors on ice. Mitochondria were isolated from the homogenates by centrifugation at 8,500*g* (pellet), 700*g* (supernatant) and 8,500*g* (pellet). The final pellets were resuspended in SHE buffer and the protein concentrations of the solution were adjusted to 1 µg µl^{-1}. The isolated mitochondrial proteins were then incubated at 37 °C in a thermomixer at 1,300 r.p.m. for 5 min, followed by further incubation for 10 min after the addition of SDS (2% final). Next, the proteins were precipitated and washed in five volumes of cold acetone to remove excess NEM. The samples were resuspended in SHE buffer with 2% SDS and 10 mM dithiothreitol, and subjected to incubation at room temperature for 15 min before the addition of an equal volume of SHE buffer containing PEG polymer conjugated to maleimide (50 mM) for another incubation at 37 °C in a thermomixer at 1,300 r.p.m. for 30 min. A second acetone precipitation was performed to remove excess the PEG–maleimide before resuspending the samples in SDS sample buffer containing 50 mM dithiothreitol and immunoblotting.

ROS measurement in brown adipocytes. The production of ROS was determined by oxidation of DHE and ratiometric assessment. Brown adipocytes were plated onto black 96-well plates and differentiated for fluorescence analysis. The cells were pre-loaded with imaging buffer (156 mM NaCl, 3 mM KCl, 2 mM $MgCl_2$, 1.25 mM KH_2PO_4 and 10 mM HEPES) containing 1 mM sodium pyruvate and 5 µM DHE. Next, 1 µM norepinephrine was added to the imaging buffer. Reduced DHE was excited at 355 nm and emission was obtained at 460 nm. Oxidized DHE was excited at 544 nm and emission was acquired at 590 nm. The ROS production was calculated as a ratio of oxidized DHE over reduced DHE.

Lipolysis assay. The BAT and iBAT depots from mice were dissected and washed with PBS. Tissue pieces of BAT and iBAT were weighed and put into a 96-well plate in KRBS buffer supplemented with 0.1% glucose and 3.5% fatty acid-free BSA at 37 °C for 2 h of pre-incubation. The tissue pieces were treated with PBS or 10 µM norepinephrine in KRBS buffer and incubated at 37 °C for another 1 h. The buffer was collected and stored at −80 °C until use. The levels of NEFA in the medium were determined using a LabAssay NEFA kit (FUJIFILM Wako Diagnostics USA Corporation) according to the manufacturer's instructions.

Antibodies. The following primary antibodies were used: anti-AIDA (Abcam, cat. no. ab199323; 1:500), anti-AIDA (Proteintech, 23724-1-AP; 1:200), anti-p-AIDA S161 (self-generated; 1:500), anti-HA (Proteintech, cat. no. 51064-2-AP; 1:3,000), anti-HA (F-7) (Santa Cruz Biotechnology, cat. no. sc7392; 1:150), anti-c-Myc (9E10) (Santa Cruz Biotechnology, cat. no. sc-40; 1:500), anti-PKA c-α (Cell Signaling Technology, cat. no. 4782; 1:1,000), anti-DYKDDDDK tag (Cell Signaling Technology, cat. no. 14793; 1:1,000), anti-β-tubulin (Cell Signaling Technology, cat. no. 2128; 1:2,000), anti-β3-tubulin (Cell Signaling Technology, cat. no. 5568; 1:1,000), anti-TH (Cell Signaling Technology, cat. no. 2792; 1:1,000), anti-p-TH S40 (Cell Signaling Technology, cat. no. 2791; 1:1,000), anti-β-actin (Cell Signaling Technology, cat. no. 3700; 1:5,000), anti-SDHA (Cell Signaling Technology, cat. no. 11998; 1:10,000), anti-GPAT3 (Proteintech, cat. no. 20603-1-AP; 1:1,000), anti-MOGAT2 (Proteintech, cat. no. 19514-1-AP; 1:1,000), anti-DGAT2 (C-15) (Santa Cruz Biotechnology, cat. no. sc-32400; 1:1,000), anti-CALNEXIN (Proteintech, cat. no. 10427-2-AP; 1:1,000), anti-SIGMAR1 (Santa Cruz Biotechnology, cat. no. sc-137075; 1:1,000), anti-HSP90 (C45G5) (Cell Signaling Technology, cat. no. 4877; 1:2,000), anti-NRF2 (Proteintech, cat. no. 16396-1-AP; 1:1,000), anti-GCLC (Proteintech, cat. no. 12601-1-AP; 1:1,000), anti-TOM20 (Proteintech, cat. no. 11802-1-AP; 1:2,000), anti-TIM23 (Proteintech, cat. no. 11123-1-AP; 1:2,000), anti-NDUFV2 (Proteintech, cat. no. 15301-1-AP; 1:10,000), anti-UQCRC2 (Proteintech, cat. no. 14742-1-AP; 1:10,000), anti-COX4 (Proteintech, cat. no. 11242-1-AP; 1:10,000), anti-ATP5A (Proteintech, cat. no. 66037-1-Ig; 1:10,000), anti-VDAC1/2 (Proteintech, cat. no. 10866-1-AP; 1:3,000), anti-ATGL (Cell Signaling Technology, cat. no. 2138; 1:1,000), anti-p-HSL S660 (Cell Signaling Technology, cat. no. 4126; 1:1,000), anti-HSL (Cell Signaling Technology, cat. no. 4107; 1:1,000), anti- UCP1 (D9D6X) (Cell Signaling Technology, cat. no. 14670; 1:200), anti-UCP1 (Abcam, cat. no. ab10983; 1:3,000) and anti-UCP1 (C-17) (Santa Cruz Biotechnology, cat. no. sc-6528; 1:200). The following secondary antibodies were used: horseradish peroxidase-conjugated goat anti-mouse IgG (Jackson ImmunoResearch, cat. no. 115-035-003; 1:5,000), horseradish peroxidase-conjugated goat anti-rabbit IgG (Jackson ImmunoResearch, cat. no. 111-035-003; 1:5,000), donkey anti-rabbit IgG secondary antibody Alexa Fluor 488 (Thermo Fisher Scientific, cat. no. A21206;

1:200) and donkey anti-mouse IgG secondary antibody Alexa Fluor 594 (Thermo Fisher Scientific, cat. no. A21203; 1:200). Detailed information is provided in Supplementary Table 3.

Statistics and reproducibility. Analysis of covariance (ANCOVA) was performed using SPSS (IBM). The other statistical analyses were performed using Prism (GraphPad Software). An unpaired two-tailed Student's *t*-test was used to determine significance between two groups of normally distributed data. Welch's correction was used for groups with unequal variances. An unpaired two-tailed Mann–Whitney test was used to determine significance between data without a normal distribution. For comparisons between multiple groups with one fixed factor, an ordinary one-way ANOVA was used, followed by Dunnett. For comparison between multiple groups with two fixed factors, an ordinary two-way ANOVA or two-way RM ANOVA was used, followed by Tukey or Sidak, as specified in the legends. Geisser–Greenhouse's correction was used where applicable. ANCOVA was used to compare the oxygen consumption and energy expenditure of the mice, while statistically controlling for the body weight of each mouse as the covariate, as indicated in the figure legends. The assumptions of homogeneity of error variances were tested using Levene's test ($P > 0.05$), the homogeneity of regression slopes assumption was tested by checking the significance of the interaction between body weight and fixed factor(s) ($P > 0.05$) and the assumption of normal distribution of residuals was also tested ($P > 0.05$). The adjusted means and s.e.m. are recorded when the analysis meets the above standards. Notably, as there is no linear correlation between the body weight and oxygen consumption of the mice or between body weight and energy expenditure in experiments with acute cold stress or CL316243 stimulation, ANCOVA was not used for analysis of the data from these experiments. For all data, differences were considered significant when $P < 0.05$. All specific statistical details can be found in the figure captions and statistics source data. At least three biological replicates were performed for all in vivo experiments. Immunoblot results were quantified using ImageJ software (National Institutes of Health) and expressed as the mean ± s.e.m. All images shown without biological replicates are representative of a minimum of two independent experiments.

Reporting Summary. Further information on research design is available in the Nature Research Reporting Summary linked to this article.

Data availability

GenBank database accession numbers: MT114182, MT114183, MT114184, MT114185, MT114186, MT114187, MT759803 and MT759804. All data that support the findings of this study are available on request from the corresponding author on reasonable request. Source data are provided with this paper.

Acknowledgements

We thank Y. Li, E. Gnaiger, T. Kuwaki, J. R. B. Lighton, E. T. Chouchani and D. Jiang for technical instruction; X. Li and X.-D. Jiang (Core Facility of Biomedical, Xiamen University) for raising the p-S161-AIDA antibody; the Xiamen University Laboratory Animal Center for the mouse in vitro fertilization service and all the other members of S.C.L. laboratory for their technical assistance. This work was supported by grants from the National Key Research and Development Project of China (grant no. 2016YFA0502001) and the National Natural Science Foundation of China (grant nos 31822027, 31871168, 31690101, 91854208 and 82088102), the Fundamental Research Funds for the Central Universities (grant nos 20720190084 and 20720200069), Project '111' sponsored by the State Bureau of Foreign Experts and Ministry of Education of China (grant no. BP2018017), the Youth Innovation Fund of Xiamen (grant no. 3502Z20206028), the Natural Science Foundation of Fujian Province of China (grant no. 2017J01364) and XMU Training Program of Innovation and Entrepreneurship for Undergraduates (grant no. 2019×0666).

Author contributions

Conceptualization: S.-C.L., S.-Y.L. and M.S. Methodology: M.S., X.-Y.H., Z.-Z.L., D.-T.L., L.S., L.Y., M.Z., C.Z., C.X., Y.W., L.P.F., H.-M.W. and S.-Y.L. Software: S.-Y.L., M.S. and X.Y.H. Formal analysis: S.-Y.L. and M.S. Investigation: M.S., X.Y.H., X.-Y.R., Y.M., X.Y.W. and S.-Y.L. Resources: T.-J.Z., G.L., J.O. and Y.-H.Z. Writing: S.-C.L., S.-Y.L. and M.S. Supervision: S.-C.L. and S.-Y.L. Project administration: S.-C.L. and S.-Y.L. Funding acquisition: S.-C.L., S.-Y.L., X.-Y.W. and Y.-H.Z.

Competing interests

The authors declare no competing interests.

Additional information

Extended data is available for this paper at https://doi.org/10.1038/s41556-021-00642-9.

Supplementary information The online version contains supplementary material available at https://doi.org/10.1038/s41556-021-00642-9.

Correspondence and requests for materials should be addressed to S.-Y.L. or S.-C.L.

Peer review information *Nature Cell Biology* thanks the anonymous reviewers for their contribution to the peer review of this work. Peer reviewer reports are available.

Reprints and permissions information is available at www.nature.com/reprints.

Uncorrected Proof

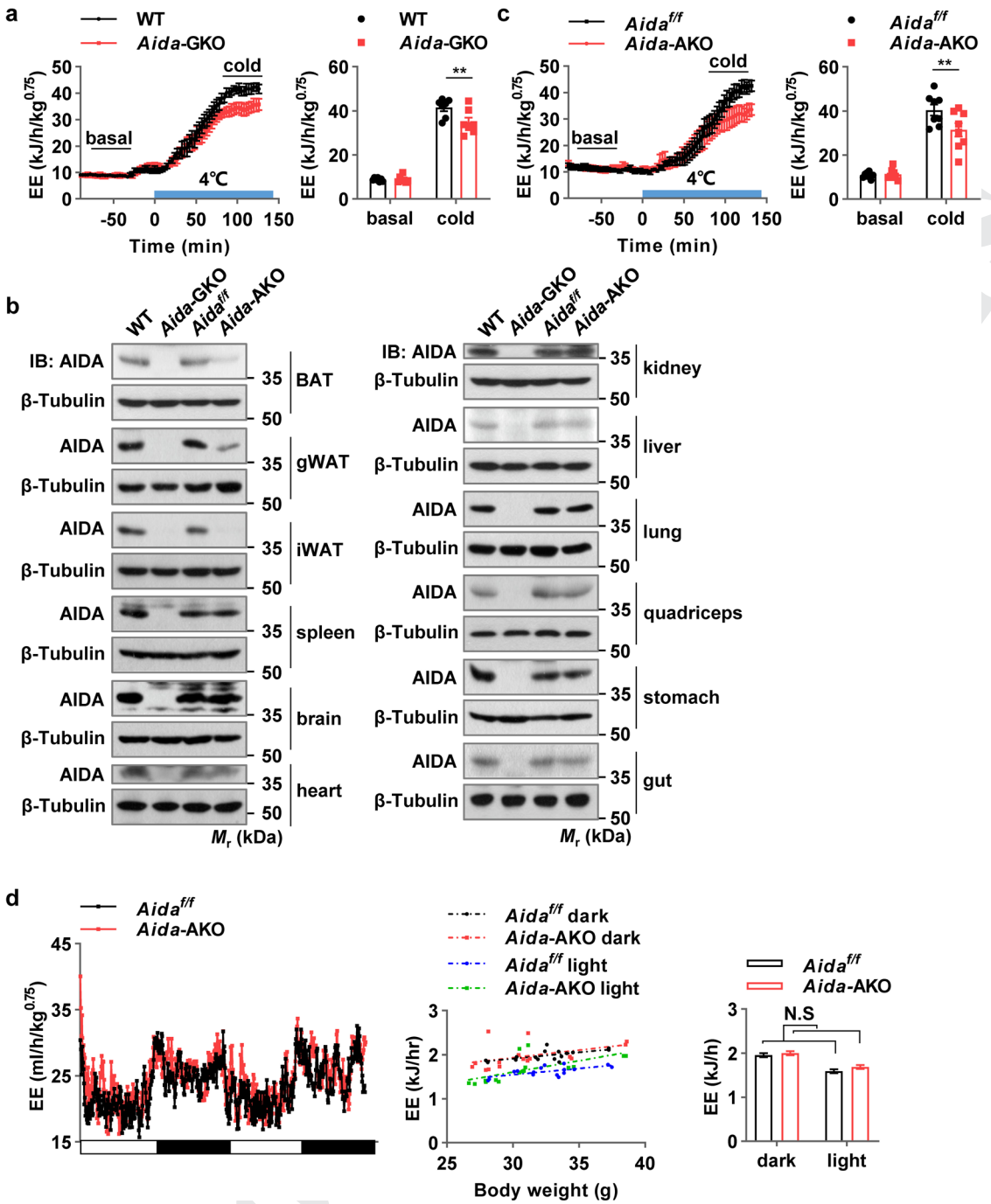

Extended Data Fig. 1 | AIDA is required for thermogenesis under cold stress. a,**c**, Energy expenditure (EE) of *Aida*-GKO (**a**) and *Aida*-AKO (**c**) mice. Data were collected from 7 (**a**) or 8 (**c**) mice per group, expressed as mean ± s.e.m. of values normalized to the body weight$^{0.75}$ (left), and average EE under basal and cold conditions, $^{**}P = 0.0044$ (**a**), $^{**}P = 0.0084$ (**c**) (two-way RM ANOVA with Sidak) (right). Basal EE was calculated as the average of 30~60 min before ambient temperature shift, EE under cold was calculated as the average of 100~130 min after temperature shift. **b**, Protein abundance of AIDA in different tissues of WT, *Aida*-GKO, *Aida*$^{f/f}$ and *Aida*-AKO mice. Data are representative of two independent experiments with similar results. **d**, EE of *Aida*$^{f/f}$ and *Aida*-AKO female mice on chow diet housed at room temperature (24 °C). Data were collected from 8 mice per group for 2 days, expressed as means of values normalized to the body weight$^{0.75}$ (left), individual EE under dark or light phase (middle), and adjusted means ± s.e.m. based on a normalized mouse weight of 31.8610 g determined by ANCOVA (right). N.S., $P = 0.134$. Uncropped blots for **b** and numerical source data for **a, c, d** are provided in Source Data Extended Data Fig. 1.

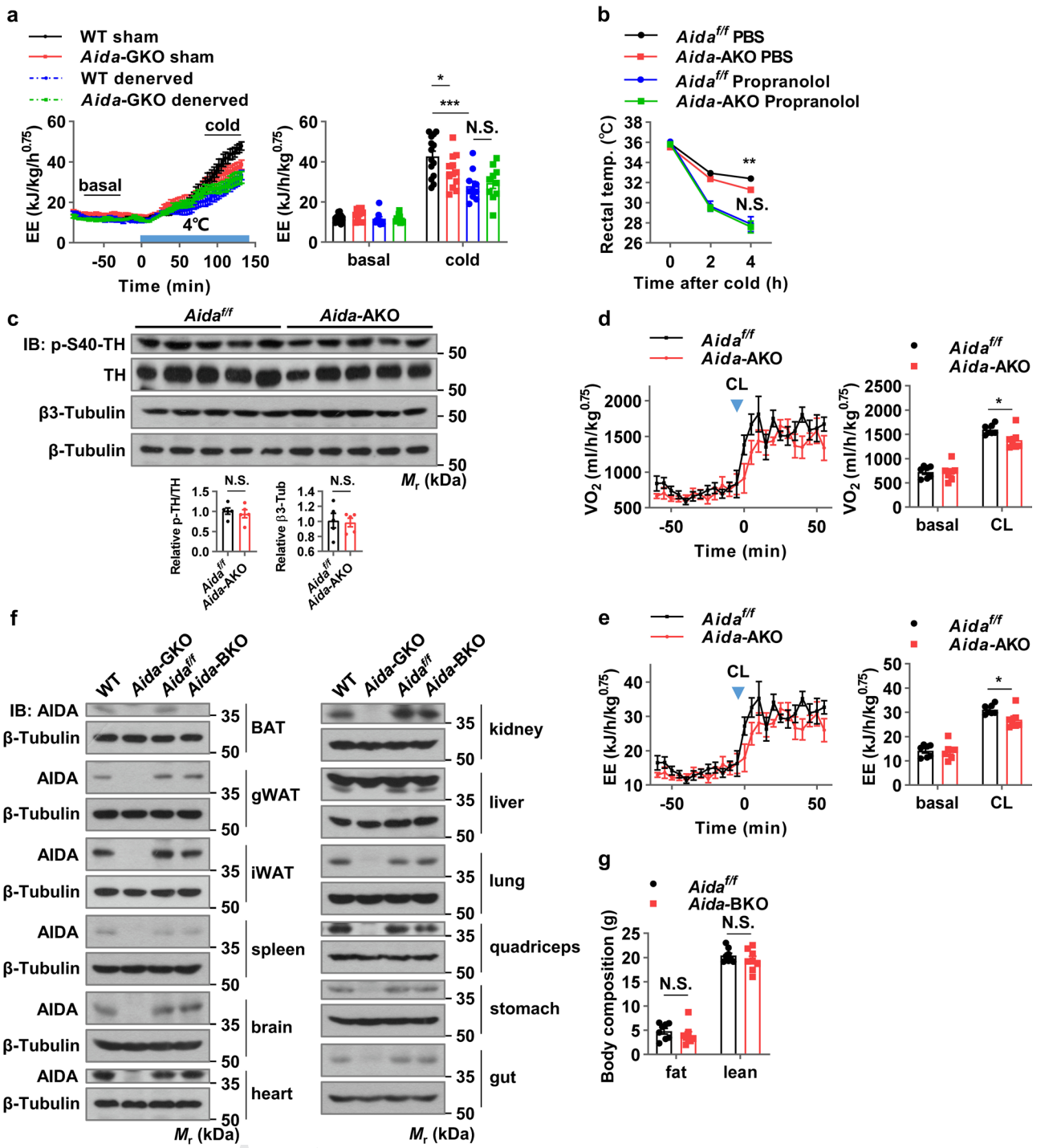

Extended Data Fig. 2 | AIDA mediates sympathetic activation of BAT. a, EE of mice two weeks after BAT denervation. WT sham $n = 14$ mice, *Aida*-GKO sham $n = 11$ mice, WT denerved or *Aida*-GKO denerved $n = 10$ mice. Mean ± s.e.m. of values normalized to the body weight$^{0.75}$ (left), individual values with mean ± s.e.m. (right). Basal, mean of 30-60 min before ambient temperature shift; cold, mean of 100-130 min after temperature shift. WT sham versus WT denerved, ***p < 0.0001; WT sham versus *Aida*-GKO sham, *$P = 0.0303$ (two-way RM ANOVA with Tukey). **b**, Cold tolerance test (CTT) of male mice pre-treated with 10 mg/kg propranolol. Mean ± s.e.m., $n = 9$ mice per group, *Aida*$^{f/f}$ PBS versus *Aida*-AKO PBS, **$P = 0.0059$ (two-way RM ANOVA with Geisser-Greenhouse correction, followed by Tukey). **c**, Immunoblotting analysis of BAT. Relative p-TH to total TH and β3-Tubulin to β-Tubulin are shown as mean ± s.e.m., $n = 5$ mice (two-tailed unpaired *t* test). **d**,**e**, OCR (**d**) and EE (**e**) of mice treated with CL316243 (1 mg/kg). Data are from 7 mice per group, presented similar as in (**a**), *$P = 0.0320$ (**d**), *$P = 0.0316$ (**e**) (two-way RM ANOVA with Sidak). Basal, the average of the 40 min period before injection; CL stimulation, the average during 40 min after CL-injection. **f**, *Aida*-knockout specificity. Data are representative of two independent experiments with similar results. **g**, Body composition of 16-week-old female mice on chow diet. Data are mean ± s.e.m., $n = 8$ mice per group (two-way RM ANOVA with Sidak). Uncropped blots for **c, f** and numerical source data for **a-e, g** are provided in Source Data Extended Data Fig. 2.

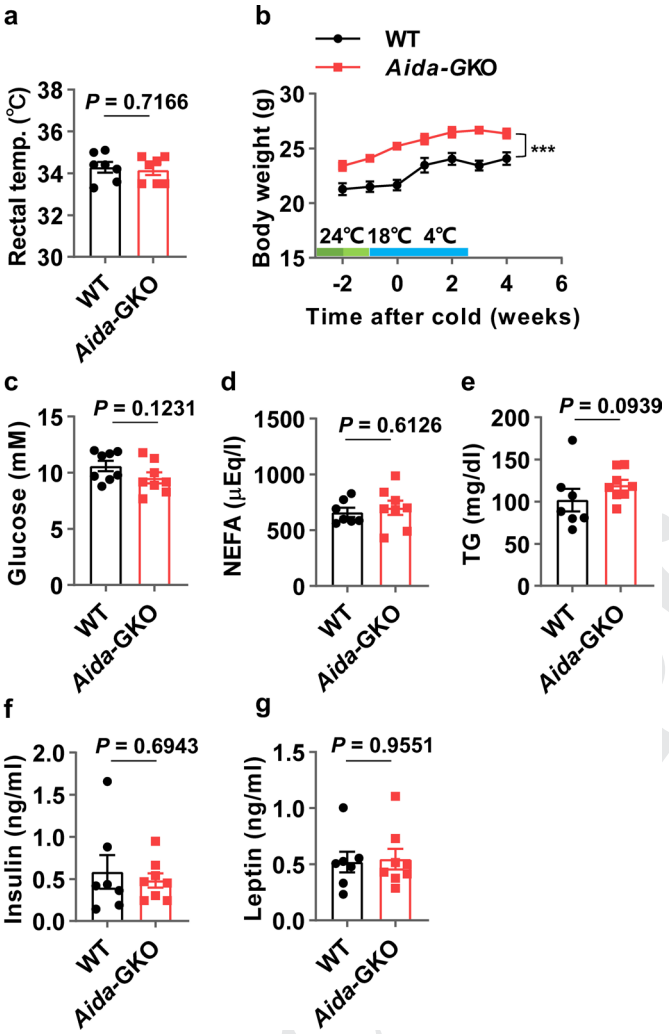

Extended Data Fig. 3 | AIDA is not required for long-term cold adaptation. a, Body temperatures of WT and *Aida*-GKO mice after a stepwise cold-adaptation (24 °C 1 week, 18 °C 1 week, 4 °C 4 weeks). Data are mean ± s.e.m., $n = 7$ mice per group, N.S., $P = 0.7166$ (two-tailed unpaired *t* test). **b**, Body weight curve of single-housed WT and *Aida*-GKO mice during stepwise cold-adaptation. Data are mean ± s.e.m., $n = 6$ mice per group. The linear regression slopes of the growth curves between WT and *Aida*-GKO mice are not significant ($P = 0.9047$). The body weights between the two groups of mice are significantly different (***$P = 0.0003$, two-way RM ANOVA with Geisser-Greenhouse correction). **c**-**g**, Blood glucose (**c**), serum non-esterified fatty acids (NEFA) (**d**), triacylglycerol (TG) (**e**), insulin (**f**) and leptin (**g**) levels of cold-adapted WT and *Aida*-GKO mice. Data are individual values with mean ± s.e.m., $n = 8$ mice per group (**c**), WT mice $n = 7$, *Aida*-GKO mice $n = 8$ (**d**-**g**) (two-tailed unpaired Mann-Whitney test). Numerical source data for **a**-**g** are provided in Source Data Extended Data Fig. 3.

Uncorrected Proofs

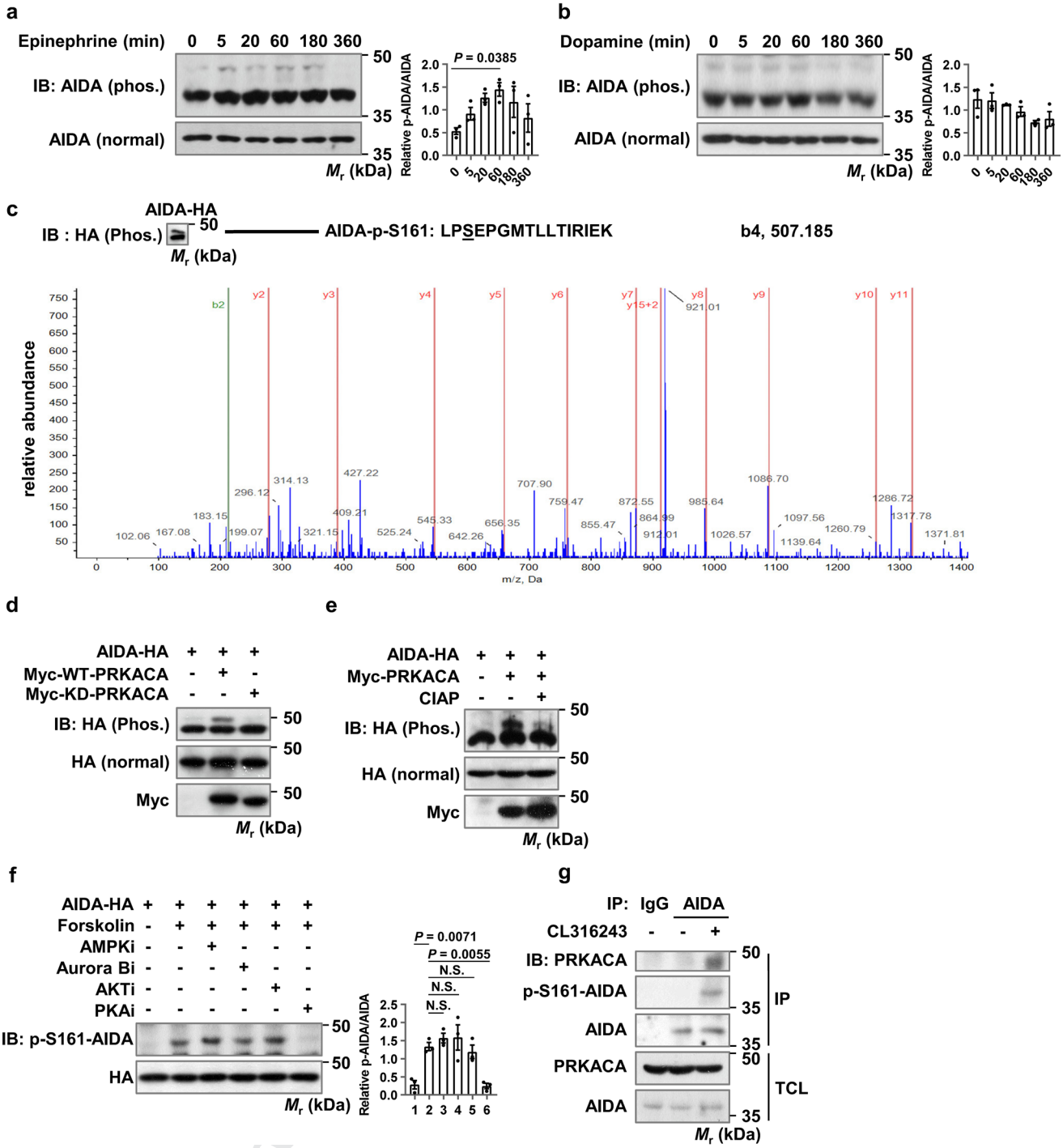

Extended Data Fig. 4 | See next page for caption.

Extended Data Fig. 4 | Phosphorylation of AIDA by PKA. a,**b**, AIDA phosphorylation after stimulation with epinephrine (**a**) or dopamine (**b**). Brown adipocytes were treated with 1 μM epinephrine or 1 μM dopamine. Cell extracts were subjected to electrophoresis using phos-tag gels (phos.) or normal gels. The relative levels of phosphorylated AIDA to total AIDA are standardized among three independent experiments and shown as mean ± s.e.m. in the right (ordinary one-way ANOVA with Dunnett). **c**, Mass spectrometry analysis of AIDA phosphorylation site. HEK293T cells expressing HA-AIDA were treated with 10 μM forskolin. The mobility-impeded band of AIDA resolved by phos-tag gel (phos.) was subjected to mass spectrometry analysis. **d**, PKA phosphorylates AIDA. HEK293T cells were transfected with WT-PRKACA (catalytic subunit of PKA) or a kinase-dead mutant of PKA (KD-PRKACA) together with HA-AIDA. The total cell lysates (TCL) were subjected to immunoprecipitation (IP) against HA. **e**, AIDA phosphorylation is eliminated by calf-intestinal alkaline phosphatase (CIAP). Lysates of HEK293T cells expressing Myc-PRKACA and HA-AIDA were subjected to IP against HA. Immunoprecipitated AIDA was treated with 2 U/μl CIAP for 1 h at 37 °C. **f**, Inhibition of PKA attenuates forskolin-induced AIDA phosphorylation. HEK293T cells transfected with HA-tagged AIDA were pre-treated with inhibitors against AMPK (Dorsomorphin, 1 μM), Aurora B (Barasertib, 1 μM), AKT (Akt inhibitor VIII, 2 μM) or PKA (H89, 30 μM) prior to stimulation with forskolin (10 μM) for 60 min. The relative intensities of p-S161-AIDA to HA-AIDA are standardized among three independent experiments and shown as mean ± s.e.m. in the right (ordinary one-way ANOVA with Dunnett). **g**, CL316243 treatment increases endogenous AIDA-Ser161 phosphorylation in WT BAT. Mice were i.p. injected with 1 mg/kg CL. 1 h post injection, BATs were homogenized and subjected to IP against endogenous AIDA. Data in **d**, **e**, **g** are representative of two independent experiments with similar results. Uncropped blots for **a, b, d-g** and numerical source data for **a, b, f** are provided in Source Data Extended Data Fig. 4.

Uncorrected proofs

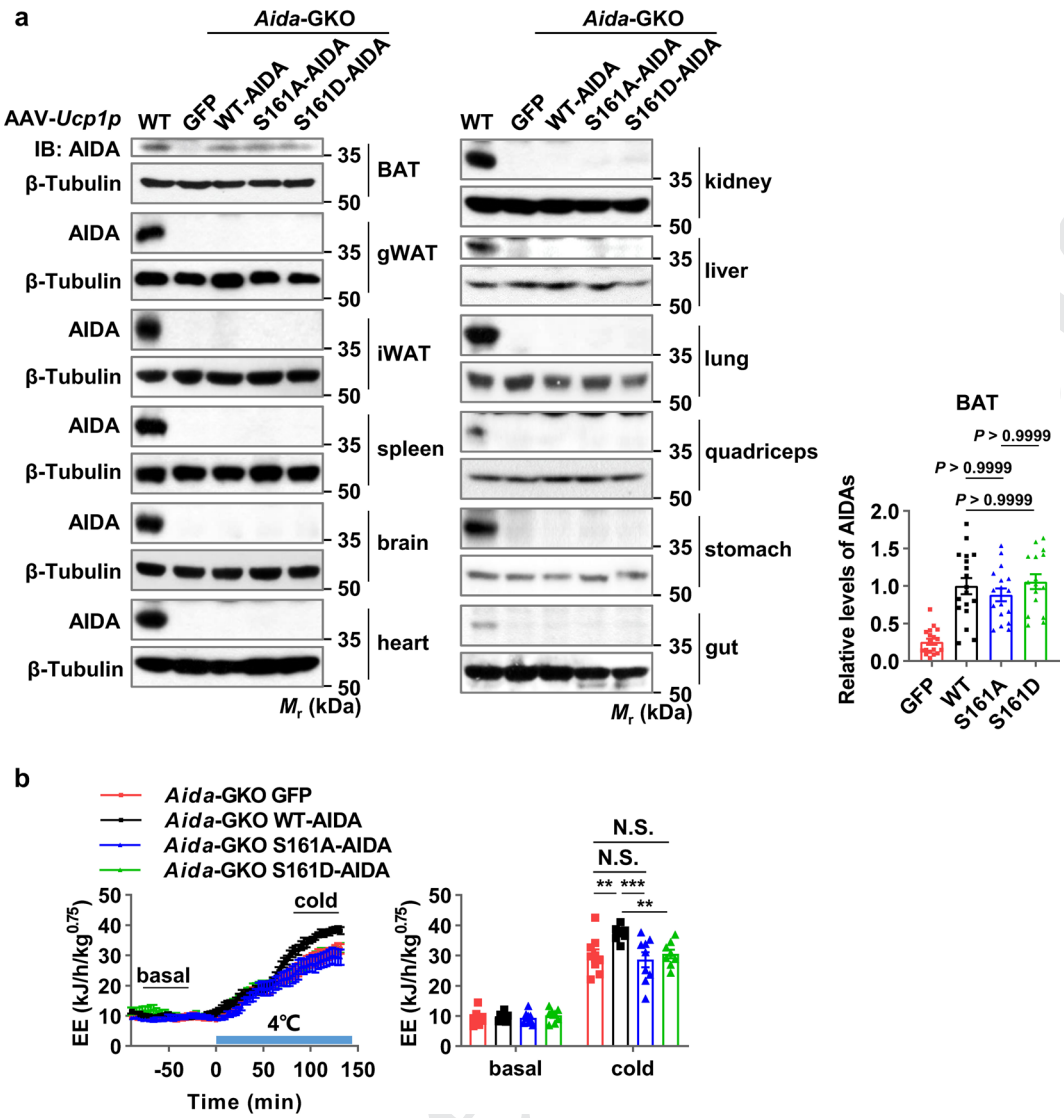

Extended Data Fig. 5 | Phosphorylation of AIDA promotes adaptive thermogenesis. a, Protein abundance of AIDA in different tissues of mice with adeno-associated virus (AAV)-mediated BAT-specific expression of AIDA. WT and *Aida*-GKO mice were injected with *Ucp1* mini-promoter and enhancer-driven AAV carrying WT-, S161A-, S161D-AIDA or GFP as a control. Blots in the left are representative samples of two independent experiments with similar results. The relative protein levels of AIDA to β-tubulin in BAT (GFP $n = 18$, WT $n = 18$, S161A $n = 17$, S161D $n = 16$ mice) are quantified and shown as mean ± s.e.m. in the right (Kruskal-Wallis test with Dunn's multiple comparisons test). **b**, EE of *Aida*-GKO mice after re-expression of WT-, S161A-, S161D-AIDA or GFP as a control to BAT under cold exposure. *Aida*-GKO GFP or *Aida*-GKO S161A-AIDA mice $n = 9$, *Aida*-GKO WT-AIDA or *Aida*-GKO S161D-AIDA mice $n = 8$. Data are mean ± s.e.m. normalized to the body weight$^{0.75}$ (upper), or average EE under basal and cold conditions (lower). Basal EE of each mice was calculated as the average of 30~60 min before ambient temperature shift, EE under cold was calculated as the average of 100~130 min after temperature shift. *Aida*-GKO GFP versus *Aida*-GKO WT-AIDA, $^{**}P = 0.0028$; *Aida*-GKO WT-AIDA versus *Aida*-GKO S161A-AIDA, $^{***}P = 0.0003$; *Aida*-GKO WT-AIDA versus *Aida*-GKO S161D-AIDA, $^{**}P = 0.0076$; N.S., not significant (two-way RM ANOVA with Tukey). Uncropped blots for **a** and numerical source data for **a, b** are provided in Source Data Extended Data Fig. 5.

Uncorrected Proofs

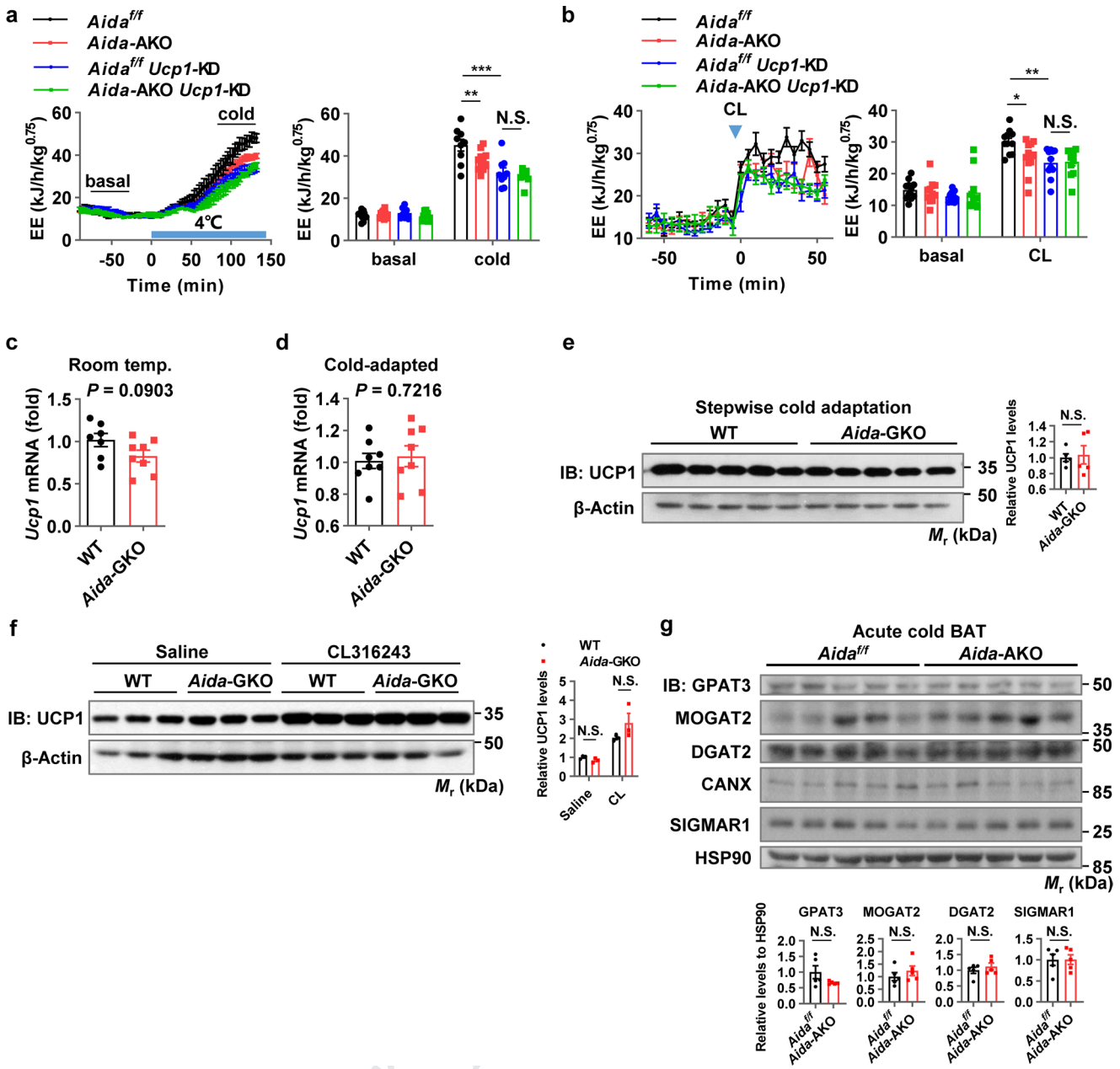

Extended Data Fig. 6 | AIDA-mediated adaptive thermogenesis is dependent on UCP1. a,**b**, EE under cold ($n = 9$ mice per group, except for *Aida*-AKO mice $n = 11$) (**a**) or i.p. CL316243 (1 mg/kg) treatment ($n = 11$ mice) (**b**). Mean ± s.e.m. of values normalized to the body weight$^{0.75}$ (left) and individual values with mean ± s.e.m. (right). Basal, average of 30~60 min before temperature shift; cold, average of 100~130 min after temperature shift. *Aida*$^{f/f}$ versus *Aida*-AKO, $^{**}P = 0.0026$; *Aida*$^{f/f}$ versus *Aida*$^{f/f}$ *Ucp1*-KD, $^{***}P < 0.0001$ (**a**). Basal and CL-stimulated values were the average of 40 min before and after CL-injection, respectively. *Aida*$^{f/f}$ versus *Aida*-AKO, $^{*}P = 0.0345$; *Aida*$^{f/f}$ versus *Aida*$^{f/f}$ *Ucp1*-KD, $^{**}P = 0.0022$ (**b**) (two-way RM ANOVA with Tukey). **c**,**d**, *Ucp1* mRNA in BAT of mice housed at room temperature (**c**) or after a stepwise cold-adaptation (**d**). Data are mean ± s.e.m., $n = 7$ WT mice, $n = 8$ *Aida*-GKO mice (**c**), $n = 8$ mice per group (**d**) (two-tailed unpaired *t* test). **e**,**f**, UCP1 in BAT of mice after a stepwise cold-adaptation (**e**), or treated with CL (1 mg/kg) daily for 5 days (**f**). Relative UCP1 levels to β-Actin are quantified and shown as mean ± s.e.m. in the right (**e**, $n = 5$ mice per group, two-tailed unpaired *t* test; **f**, $n = 3$ mice, ordinary two-way ANOVA, Tukey). **g**, ERAD-associated proteins in BAT. $n = 5$ mice. Relative protein levels to HSP90 are quantified and shown as mean ± s.e.m. below (two-tailed unpaired *t* test with Welch's correction). Uncropped blots for **e-g** and numerical source data for **a-g** are provided in Source Data Extended Data Fig. 6.

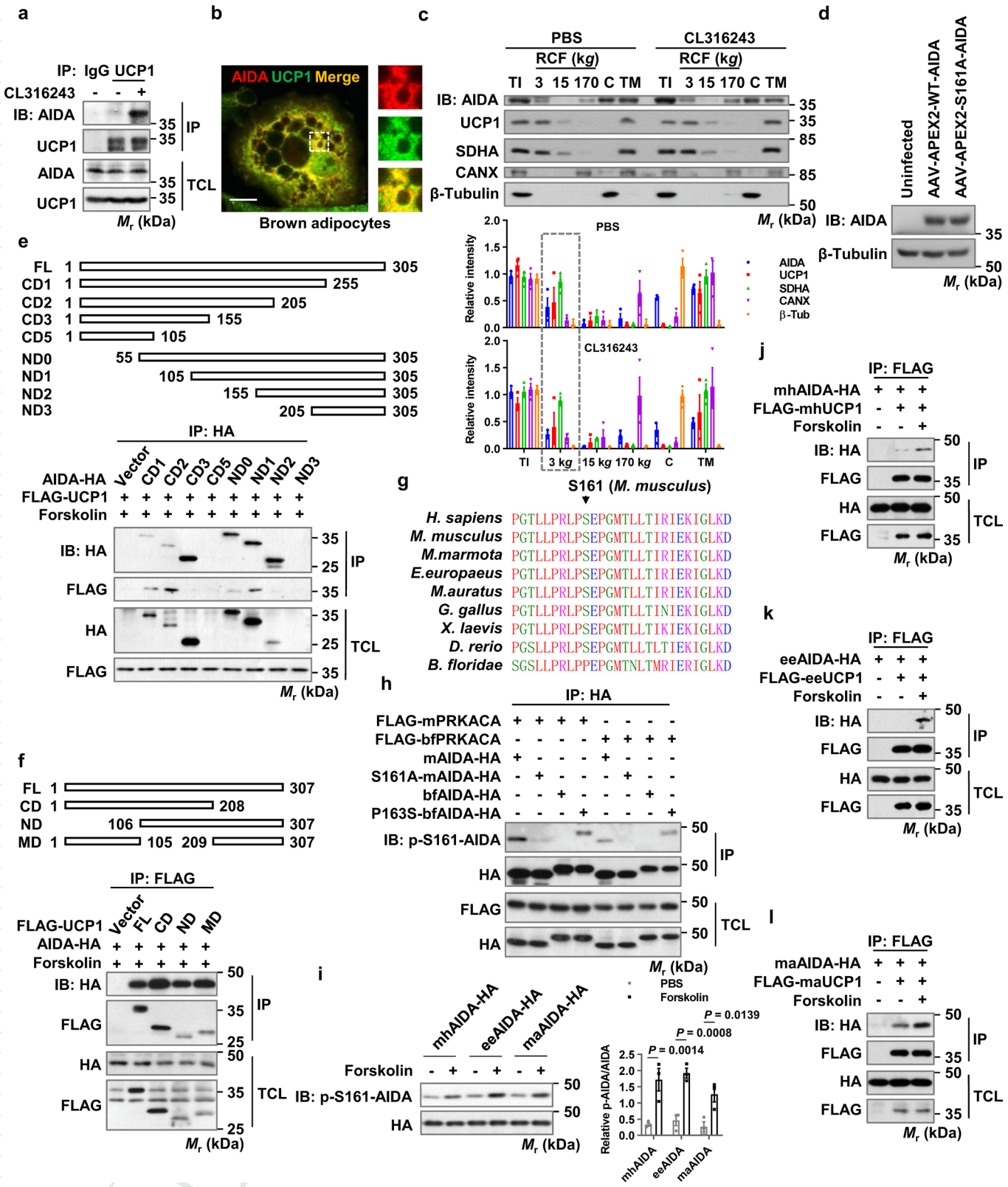

Extended Data Fig. 7 | See next page for caption.

Extended Data Fig. 7 | AIDA interacts with UCP1. a, Co-IP of endogenous AIDA and UCP1 using BAT from WT mice treated with PBS or CL316243 (1 mg/kg) for 1 h. **b**, Immunofluorescence analysis of localization of ectopically expressed AIDA-HA and endogenous UCP1 in primary brown adipocytes. Red, AIDA; green, UCP1. Scale bar, 10 μm. **c**, Immunoblotting analysis of the fractionation patterns of AIDA and UCP1 in BAT from WT mice injected with PBS or CL316243 (1 mg/kg) for 1 h. Relative intensities of AIDA, UCP1, SDHA, CANX and β-Tubulin are quantified (lower). **d**, Validation of expression of APEX2-AIDA in BAT from cold-stimulated mice. **e**,**f**, Determination of UCP1-binding domain in AIDA (**e**) and AIDA-binding domain in UCP1 (**f**). FL, full length; CD, C-terminal deletion; ND, N-terminal deletion; MD, middle deletion. Experiment performed once. **g**, Alignment of AIDA Ser161 (in mouse) residue and the flanking amino acid residues in different species. **h**, Alteration of Pro163 to Ser of *Branchiostoma floridae* (bf) AIDA renders it a substrate for PKA. HEK293T cells were transfected with WT-bfAIDA or P163S-bfAIDA together with mPRKACA or bfPRKACA. Cells were lysed and subjected to IP against HA. **i**, PKA phosphorylates AIDA of marmot (mh), hedgehog (ee) and hamster (ma). HEK293T cells were transfected with HA-AIDA. Following 1 h treatment of forskolin (10 μM), the cells were lysed and subjected to IP against HA. The relative intensities of p-S161-AIDA to total AIDA are standardized among three independent experiments and shown as mean ± s.e.m. in the right (ordinary two-way ANOVA with Sidak). **j**-**l**, Interaction between AIDA and UCP1 of marmot (**j**), hedgehog (**k**) and hamster (**l**) after adrenergic stimulation. HEK293T cells were transfected with AIDA and UCP1. After 1 h forskolin (10 μM) treatment, the cells were lysed and subjected to IP against FLAG. Data in **a**-**f**, **h**, **j**-**l** are representative of two independent experiments with similar results. Uncropped blots for **a, c-f, h-l** and numerical source data for **c, i** are provided in Source Data Extended Data Fig. 7.

Uncorrected proofs

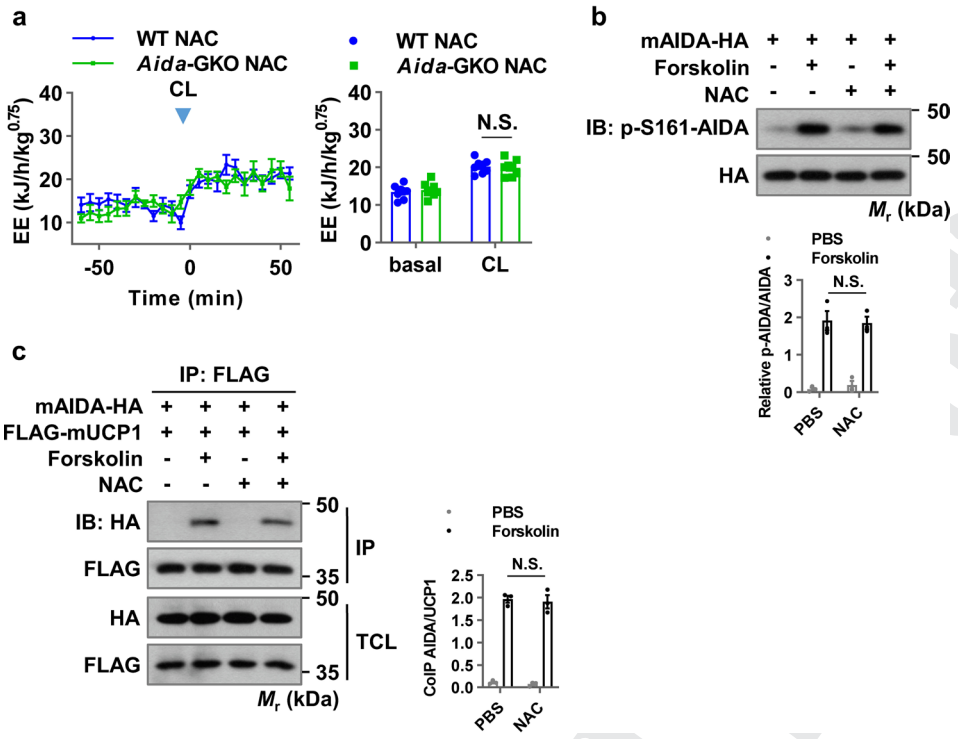

Extended Data Fig. 8 | ROS production and the phosphorylation of AIDA are separate events downstream of adrenergic stimulation. a, EE of mice before and after CL316243 injection pre-treated with NAC. Mice were i.p. injected with NAC (500 mg/kg) 10 min before injection of CL316243 (1 mg/kg). $n = 8$ mice. Data are shown as mean ± s.e.m. of values normalized to the body weight$^{0.75}$ (left), and individual normalized values before and after CL-injection (right). N.S., $P = 0.9391$ (two-way RM ANOVA with Sidak). **b**,**c**, Effect of NAC (10 mM) pre-treatment on AIDA phosphorylation (**b**) and the interaction between AIDA and UCP1 (**c**) after forskolin (10 μM) stimulation in HEK293T cells. The relative intensities of p-S161-AIDA to total AIDA (**b**) and immunoprecipitated AIDA to UCP1 (**c**) are standardized among three independent experiments and shown as mean ± s.e.m. in the right (ordinary two-way ANOVA with Tukey). Uncropped blots for **b, c** and numerical source data for **a-c** are provided in Source Data Extended Data Fig. 8.

Uncorrected Proofs

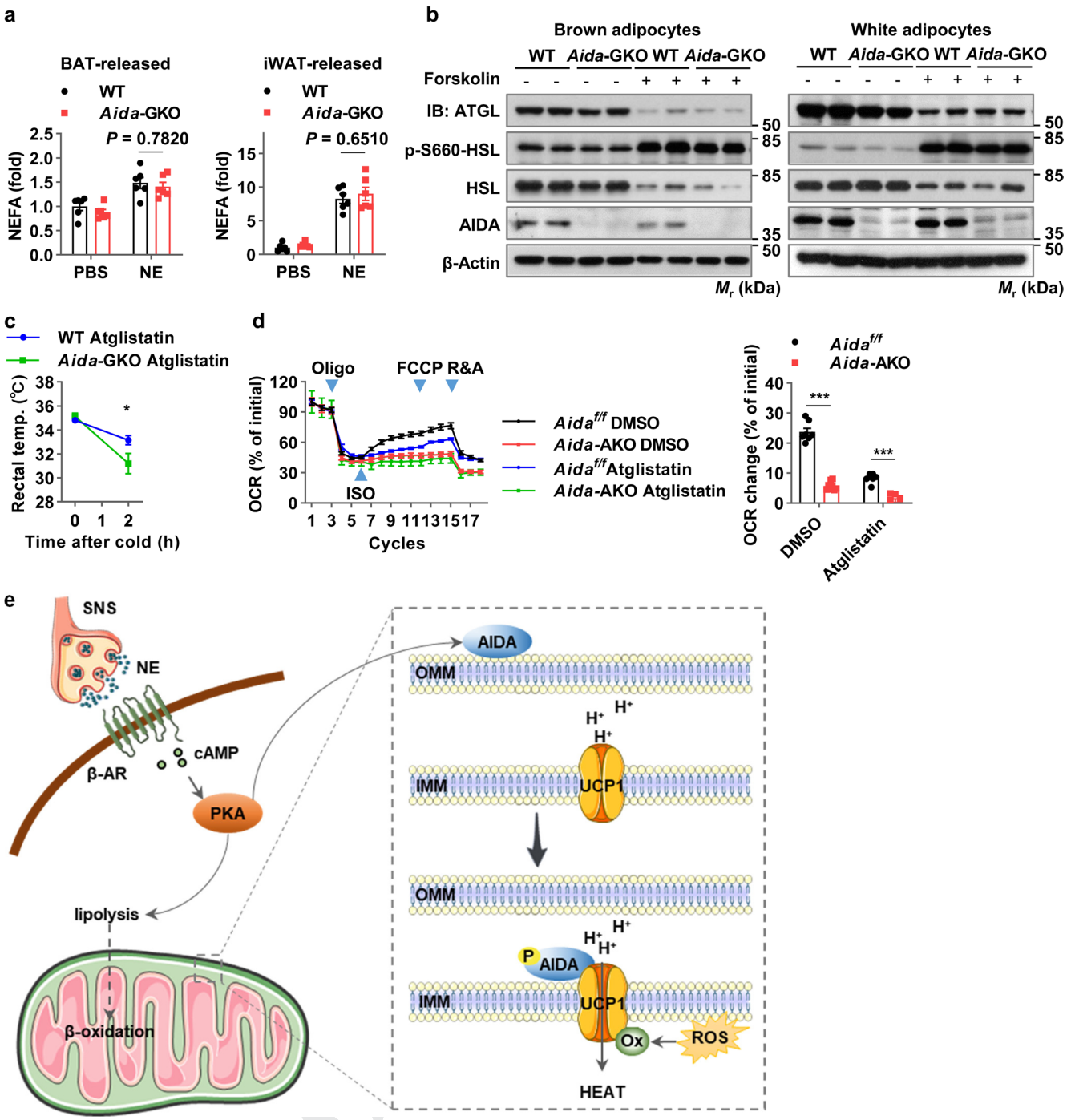

Extended Data Fig. 9 | Activation of UCP1 by fatty acids is independent of AIDA. a, Fold change of NEFA released from BAT (left) or iWAT (right) of mice in response to NE (10 μM). Data are mean ± s.e.m., $n = 6$ BATs or iWATs per group (ordinary two-way ANOVA with Sidak). **b**, Immunoblotting analysis of lipases in mice-derived brown adipocytes (left) and white adipocytes (right) treated with forskolin (10 μM). Adipocytes are derived from $n = 2$ mice. **c**, CTT of mice pre-treated with ATGL inhibitor. Mice were i.p. injected with Atglistatin (50 μM/kg) at 10 min before cold exposure. Atglistatin was dissolved in 25% HCl. Atglistatin-HCl complex was obtained via evaporating excess HCl and dissolved in PBS containing 0.25% castor oil. Data are mean ± s.e.m., $n = 8$ mice per group, $^*P = 0.0193$ (two-way RM ANOVA with Sidak). **d**, OCR of brown adipocytes from *Aida*$^{f/f}$ and *Aida*-AKO mice. Brown adipocytes were pre-treated with DMSO or Atglistatin (40 μM) 1 h before test. OCR at each cycle is calculated as the percentage of initial OCR, shown as mean ± s.e.m., *Aida*$^{f/f}$ brown adipocytes are from $n = 7$ mice, *Aida*-AKO brown adipocytes are from $n = 8$ mice. Graph on the right indicates the quantification of changes of ISO-induced mitochondrial uncoupling respiration rates over basal mitochondrial uncoupling respiration rates, data are mean ± s.e.m., $^{***}P < 0.0001$ (ordinary two-way ANOVA with Tukey). **e**, A schematic model showing that adrenergic signalling leads to phosphorylation of AIDA by PKA, phosphorylated AIDA in turn interacts with and promotes oxidation of UCP1, promoting adaptive thermogenesis by UCP1. Several elements of this image were adopted and modified from Servier Medical Art by Servier (https://smart.servier.com/) licensed under a Creative Commons Attribution 3.0 Unported License (https://creativecommons.org/licenses/by/3.0/). Uncropped blots for **b** and numerical source data for **a, c, d** are provided in Source Data Extended Data Fig. 9.